

Global Biogeochemical Cycles[®]

RESEARCH ARTICLE

10.1029/2024GB008310

Special Collection:

REgional Carbon Cycle
Assessment and Processes -2
(RECCAP2)

Key Points:

- Total North American net greenhouse-gas (GHG) emissions for 2010–2019 range from 6,132 to 9,060 TgCO₂-eq yr⁻¹
- Lateral aquatic and trade fluxes, double counting, and definitions are the main sources of uncertainty for reconciling GHG estimates
- Net-GHG emissions have decreased from 2000 to 2019 due to fossil emissions, and natural ecosystem removals appear to be stable or increased

Supporting Information:

Supporting Information may be found in the online version of this article.

Correspondence to:

B. Poulter,
benjamin.poulter@nasa.gov

Citation:

Poulter, B., Murray-Tortarolo, G., Hayes, D. J., Ciais, P., Andrew, R. M., Bastos, A., et al. (2025). The North American greenhouse gas budget: Emissions, removals, and integration for CO₂, CH₄, and N₂O (2010–2019): Results from the Second REgional Carbon Cycle Assessment and Processes Study (RECCAP2). *Global Biogeochemical Cycles*, 39, e2024GB008310. <https://doi.org/10.1029/2024GB008310>













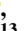
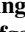

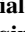


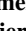

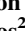


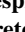
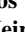



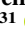
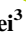










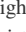
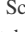
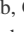

Received 24 JUL 2024

Accepted 19 MAR 2025

Author Contributions:

Conceptualization: Benjamin Poulter, Guillermo Murray-Tortarolo, Daniel J. Hayes, Philippe Ciais, Ana Bastos, David Butman, Josep G. Canadell, Robert B. Jackson, Werner A. Kurz, Anna M. Michalak, John Miller, Peter

The North American Greenhouse Gas Budget: Emissions, Removals, and Integration for CO₂, CH₄, and N₂O (2010–2019): Results From the Second REgional Carbon Cycle Assessment and Processes Study (RECCAP2)

Benjamin Poulter¹ , Guillermo Murray-Tortarolo² , Daniel J. Hayes³ , Philippe Ciais⁴ , Robbie M. Andrew⁵ , Ana Bastos⁶ , Brendan Byrne⁷ , David Butman⁸ , Josep G. Canadell⁹ , Abhishek Chatterjee⁷ , Grant Domke¹⁰ , Andrew Feldman^{1,11} , Kelsey Foster^{12,13} , Neha Hunka¹⁴ , Robert B. Jackson¹³ , Werner A. Kurz¹⁵ , Ayia Lindquist^{1,16} , Maodian Liu^{17,18} , Ingrid Luijckx¹⁹ , Arnaud Mialon²⁰ , Anna M. Michalak^{12,13} , John Miller²¹ , Wolfgang A. Obermeier²² , Naiqin Pan²³ , James T. Randerson²⁴ , Peter A. Raymond¹⁷ , Pierre Regnier²⁵ , Laure Resplandy²⁶ , Gerard Rocher-Ros²⁷ , Nemesio Rodriguez-Fernandez²⁰ , Judith Rosentreter²⁸ , Julio César Salazar-Neira²⁰ , Suzanne E. Tank²⁹ , Hanqin Tian²³ , Rodrigo Vargas³⁰ , Yohanna Villalobos³¹ , Jonathan A. Wang³² , Xinyuan Wei³ , Kimberly P. Wickland³³ , Christopher Williams³⁴ , Lisamarie Windham-Myers³⁵ , Christopher Woodall³⁶ , Qing Ying^{1,11} , and Zhen Zhang^{1,11} 

¹NASA Goddard Space Flight Center, Earth Sciences Division, Biospheric Sciences Lab, Greenbelt, MD, USA, ²Instituto de Investigaciones en Ecosistemas y Sustentabilidad, Universidad Nacional Autónoma de México. UNAM. Campus Morelia, Morelia, Mexico, ³School of Forest Resources, University of Maine, Orono, ME, USA, ⁴Laboratoire des Sciences du Climat et de l'Environnement, CEA-CNRS-UVSQ-U.P.Saclay, Gif sur Yvette, France, ⁵CICERO Center for International Climate Research, Oslo, Norway, ⁶Institute for Earth System Science and Remote Sensing, Leipzig University, Leipzig, Germany, ⁷Jet Propulsion Laboratory, California Institute of Technology, Pasadena, CA, USA, ⁸School of Environmental and Forest Sciences, University of Washington, Seattle, WA, USA, ⁹CSIRO Environment, Canberra, ACT, Australia, ¹⁰Northern Research Station, USDA Forest Service, St. Paul, MN, USA, ¹¹Earth System Science Interdisciplinary Center, University of Maryland, College Park, MD, USA, ¹²Department of Global Ecology, Carnegie Institution for Science, Stanford, CA, USA, ¹³Department of Earth System Science, Stanford University, Stanford, CA, USA, ¹⁴Department of Geographical Sciences, University of Maryland, College Park, MD, USA, ¹⁵Natural Resources Canada, Canadian Forest Service, Victoria, BC, Canada, ¹⁶NASA Goddard Space Flight Center, Science Systems and Applications, Greenbelt, MD, USA, ¹⁷School of the Environment, Yale University, New Haven, CT, USA, ¹⁸Ministry of Education Laboratory of Earth Surface Process, College of Urban and Environmental Science, Peking University, Beijing, China, ¹⁹Environmental Sciences Group, Wageningen University, Wageningen, The Netherlands, ²⁰CNES/IRD/CNRS/INRAe, CESBIO, University of Toulouse, Toulouse, France, ²¹NOAA Global Monitoring Laboratory, Boulder, CO, USA, ²²Department of Geography, Ludwig Maximilian University Munich, Munich, Germany, ²³Department of Earth and Environmental Sciences, Center for Earth System Science and Global Sustainability, Boston College, Schiller Institute for Integrated Science and Society, Chestnut Hill, MA, USA, ²⁴Department of Earth System Science, University of California, Irvine, CA, USA, ²⁵Department of Geosciences, Environment and Society, Biogeochemistry and Modelling of the Earth System (BGEOSYS), Université Libre de Bruxelles, Brussels, Belgium, ²⁶Department of Geosciences, Princeton University, Princeton, NJ, USA, ²⁷Department of Forest Ecology and Management, Swedish University of Agricultural Sciences, Umeå, Sweden, ²⁸Center for Coastal Biogeochemistry, Faculty of Science and Engineering, Southern Cross University, Lismore, NSW, Australia, ²⁹Department of Biological Sciences, University of Alberta, Edmonton, AB, Canada, ³⁰Department of Plant and Soil Sciences, University of Delaware, Newark, DE, USA, ³¹Department of Physical Geography and Ecosystem Science (INES), Lund University, Lund, Sweden, ³²School of Biological Sciences, University of Utah, Salt Lake City, UT, USA, ³³Geosciences and Environmental Change Science Center, United States Geological Survey, Boulder, CO, USA, ³⁴Graduate School of Geography, Clark University, Worcester, MA, USA, ³⁵United States Geological Survey Water Resources Mission Area, Menlo Park, CA, USA, ³⁶USDA Forest Service, Northern Research Station, Forest Inventory and Analysis Program, Durham, NH, USA

Abstract Accurate accounting of greenhouse-gas (GHG) emissions and removals is central to tracking progress toward climate mitigation and for monitoring potential climate-change feedbacks. GHG budgeting and reporting can follow either the Intergovernmental Panel on Climate Change methodologies for National Greenhouse Gas Inventory (NGHI) reporting or use atmospheric-based “top-down” (TD) inversions or process-based “bottom-up” (BU) approaches. To help understand and reconcile these approaches, the Second Regional Carbon Cycle Assessment and Processes study (RECCAP2) was established to quantify GHG

© 2025 The Author(s).

This is an open access article under the terms of the [Creative Commons Attribution-NonCommercial License](https://creativecommons.org/licenses/by-nc/4.0/), which permits use, distribution and reproduction in any medium, provided the original work is properly cited and is not used for commercial purposes.

A. Raymond, Suzanne E. Tank,
Rodrigo Vargas, Kimberly P. Wickland,
Christopher Williams,
Lisamarie Windham-Myers

Data curation: Benjamin Poulter, Robbie M. Andrew, Brendan Byrne, David Butman, Abhishek Chatterjee, Grant Domke, Andrew Feldman, Kelsey Foster, Neha Hunka, Werner A. Kurz, Ayia Lindquist, Maodian Liu, Ingrid Luijckx, Arnaud Mialon, John Miller, Wolfgang A. Obermeier, Naiqin Pan, James T. Randerson, Pierre Regnier, Laure Resplandy, Gerard Rocher-Ros, Nemesio Rodriguez-Fernandez, Judith Rosentreter, Julio César Salazar-Neira, Suzanne E. Tank, Hanqin Tian, Rodrigo Vargas, Jonathan A. Wang, Xinyuan Wei, Kimberly P. Wickland, Lisamarie Windham-Myers, Christopher Woodall, Zhen Zhang

Formal analysis: Benjamin Poulter, Daniel J. Hayes, Robbie M. Andrew, Brendan Byrne, Grant Domke, Ingrid Luijckx, Wolfgang A. Obermeier, Naiqin Pan, Peter A. Raymond, Pierre Regnier, Judith Rosentreter, Hanqin Tian, Christopher Woodall, Qing Ying

Investigation: Benjamin Poulter

Methodology: Benjamin Poulter, Philippe Ciais, Ingrid Luijckx, Peter A. Raymond, Judith Rosentreter, Yohanna Villalobos

Supervision: Benjamin Poulter

Visualization: Benjamin Poulter, Qing Ying

Writing – original draft:

Benjamin Poulter, Daniel J. Hayes, Abhishek Chatterjee, Andrew Feldman, Ingrid Luijckx, Pierre Regnier, Judith Rosentreter, Suzanne E. Tank, Hanqin Tian, Rodrigo Vargas, Yohanna Villalobos, Christopher Woodall

Writing – review & editing:

Benjamin Poulter, Daniel J. Hayes

emissions and removals for carbon dioxide (CO₂), methane (CH₄) and nitrous oxide (N₂O), for ten-land and five-ocean regions for 2010–2019. Here, we present the results for the North American land region (Canada, the United States, Mexico, Central America and the Caribbean). For 2010–2019, the NGHGI reported total net-GHG emissions of 7,270 TgCO₂-eq yr⁻¹ compared to TD estimates of 6,132 ± 1,846 TgCO₂-eq yr⁻¹ and BU estimates of 9,060 ± 898 TgCO₂-eq yr⁻¹. Reconciling differences between the NGHGI, TD and BU approaches depended on (a) accounting for lateral fluxes of CO₂ along the land-ocean-aquatic continuum (LOAC) and trade, (b) correcting land-use CO₂ emissions for the loss-of-additional-sink capacity (LASC), (c) avoiding double counting of inland water CH₄ emissions, and (d) adjusting area estimates to match the NGHGI definition of the managed-land proxy. Uncertainties remain from inland-water CO₂ evasion, the conversion of nitrogen fertilizers to N₂O, and from less-frequent NGHGI reporting from non-Annex-1 countries. The RECCAP2 framework plays a key role in reconciling independent GHG-reporting methodologies to support policy commitments while providing insights into biogeochemical processes and responses to climate change.

Plain Language Summary Climate change is driven by increasing atmospheric greenhouse gases from human activities. Reducing the emissions (or increasing removals) of anthropogenic greenhouse gas emissions is a key component of climate mitigation policies. The REgional Carbon Cycle Assessment and Processes (RECCAP2) study was developed to quantify greenhouse gas emissions for carbon dioxide, methane and nitrous oxide, and for key land and ocean regions to help advance science and policy needs. The North American region, presented in this paper, uses a wide range of data to develop greenhouse-gas budgets following top-down and bottom-up approaches, and compares these with the national greenhouse gas inventories submitted to the United Nations Framework Convention on Climate Change. We pay particular attention to reconciling differences by quantifying lateral fluxes of carbon from aquatic and trade processes, by isolating cases of double counting of inland water emissions, and by evaluating definitions associated with land cover change emissions and the “managed lands proxy.” Combined, we provide the regional and sub-regional GHG budget and comparison for 2000–2009 and 2010–2019 for the three gases and their global warming potential equivalent.

1. Introduction

Measurement and monitoring of greenhouse-gas (GHG) emissions and removals is necessary for developing GHG budgets to support climate policy and also to help detect climate impacts and potential climate feedbacks on the carbon cycle. From a scientific perspective, the development of GHG budgets provides an opportunity for a detailed understanding of biogeochemical flows and their sensitivity to climate variability and trends. And from a policy perspective, accurate accounting of anthropogenic emissions and removals is a key reporting component to support climate mitigation efforts.

The REgional Carbon Cycle Assessment and Processes study (RECCAP1), first established in 2008, developed carbon dioxide (CO₂) budgets for 10-land and 5-ocean regions for the period 1990–2009 (Canadell et al., 2011). RECCAP1 was designed to improve our scientific understanding of the carbon cycle, and led to the key finding that lateral flows of carbon along the land-ocean aquatic continuum (LOAC) and from carbon embodied in the trade of wood and crop products need to be quantified accurately for reconciling activity-based (i.e., bottom up) and atmospheric-based (i.e., top down) methods (Ciais et al., 2021). In 2017, RECCAP2 was launched to develop multi-GHG budgets for the same ten-land regions for the period 2010–2019, including two special focus regions, the permafrost and polar regions (Poulter et al., 2022). RECCAP2 takes place in an era following RECCAP1 where a range of new policies have been established to mitigate GHG gas emissions.

This paper presents the GHG budget for the North American region, which includes Canada, the United States, Mexico, Central America and the Caribbean. Findings from RECCAP1 estimated North American fossil-fuel emissions (for 1990–2009) as 6,300 TgCO₂ yr⁻¹ and found that emissions are offset by 1,000 to 3,300 TgCO₂ yr⁻¹ due to removals from the land sector (King et al., 2015). The Second State of the Carbon Cycle Report (SOCCR-2; Birdsey et al., 2018), covering the years 2004–2013, also estimated North American natural and managed ecosystem removals of ~2,224–2,565 TgCO₂ yr⁻¹ partially offsetting annual fossil fuel emissions of 6,510 TgCO₂ yr⁻¹ (Hayes et al., 2018). More recently, atmospheric-based estimates from the Orbiting Carbon Observatory-2 Model Intercomparison (OCO2-MIP), suggest an increase in land removals of 2,730–

3,154 TgCO₂ yr⁻¹ (Byrne et al., 2023) for the period 2015–2019. For non-CO₂ gases, data from the Global Methane (CH₄) Budget (2008–2017) and Global Nitrous Oxide (N₂O) Budget (2007–2016), coordinated by the Global Carbon Project, estimate North America to be a source of 78–112 TgCH₄ yr⁻¹ (Stavert et al., 2022) and 1.3 to 1.7 TgN₂O yr⁻¹ (Tian et al., 2020, 2024).

Guidance for RECCAP2 was provided by Ciais et al. (2022) in the form of a framework for quantifying the flows of CO₂ and reconciling bottom-up (BU) and top-down (TD) approaches. For non-CO₂ gases, the RECCAP2 teams following the Global Carbon Project's CH₄ and N₂O Budget frameworks. For each of the three gases, particular attention was paid to agreement between the BU and TD approaches by quantifying lateral fluxes, using appropriate definitions, and avoiding double counting. Data sets along the LOAC continuum were developed for inland waters by Lauerwald et al. (2023a, 2023b), and for estuaries and coastal systems by Rosentreter et al. (2023) and lateral fluxes determined following the approach of Regnier et al. (2022) and Liu et al. (2024). Definitions for the land-sector were characterized as appropriate for the managed-land proxy (McGlynn et al., 2022; Ogle et al., 2018) and for comparing process-based and bookkeeping approaches while accounting for the loss of additional sink capacity (Schwingshackl et al., 2022). Double counting is discussed in particular for CH₄ emissions from vegetated wetlands and inland waters, which remain challenging to partition due to observational data and model limitations (Saunio et al., 2020).

The RECCAP2 study encourages the use of multiple quasi-independent data sources to help characterize uncertainties and to also provide unique insights into different underlying processes for GHG emissions and removals. For this study, data from direct measurements of biomass and atmospheric concentrations are used with indirect measurements from satellite retrievals and process-based models. In addition, data from the annual National Inventory Reports (NIR) are used for Canada and the United States and from the periodic Biennial Update Reports (BUR) are used for Mexico, Central America and the Caribbean. These inventories follow the Intergovernmental Panel on Climate Change guidelines to estimate sectoral emissions and removals for energy, industrial processes and product uses (IPPU), agriculture, land use, land-use change and forestry (i.e., AFOLU), and waste (Deng et al., 2022).

Since the first RECCAP was completed in 2012, climate change, climate extremes, land-cover and land-use change, and climate-mitigation policies have affected North American GHG emissions and removals (Crimmins et al., 2023). Since 1961, air temperature has warmed across North America by +0.29°C per decade, and precipitation has increased by +0.34 mm per decade, but with smaller increases over Canada. Across the US, Landsat analysis from 1985 to 2016 suggests land-cover change was primarily driven by an expansion in urban areas causing declines in forest carbon and cropland cover (Auch et al., 2022). For the rest of North America, land-use statistics, that is, US Department of Agriculture's National Resources Inventory (Nusser, 2012), show similar increases in urban-area expansion along with declining forest and cropland. The North American carbon cycle is also responding to climate changes at interannual and decadal timescales (Hu et al., 2019; Murray-Tortarolo et al., 2022). At the same time, rapid expansion in oil and gas activities, livestock populations, and intensification in fertilizer use has led to increasing CH₄ and N₂O emissions (Alvarez et al., 2018; Tian et al., 2020).

RECCAP2 thus provides a critical opportunity to quantify anthropogenic and climatic effects on the net radiative balance of GHGs in North America (i.e., CO₂-eq) across all sectors. We also include a budget for 2000–2009 in addition to 2010–2019 to evaluate decadal GHG changes. In the following, we quantify the emissions and removals for the three main GHGs for North America and its four subregions. We present independent flux-based and stock-change accounting to estimate the CO₂ budget for North American territorial and non-territorial consumption, and a flux-based approach only for the CH₄ and N₂O budgets. We convert the fluxes of the three gases to their global warming potentials using the GWP100 (IPCC, 2023) to evaluate the total GWP of the North American continent and its subregions considering the imbalance between atmospheric GHG emissions and removals.

2. Methods

2.1. Study Area

The study area encompasses the RECCAP2-defined North American land region, which together represents about 17% of global land area. The GHG budgets are presented for the entire region and also separately for the four subregions: Canada, the United States of America, including Alaska, Hawaii and territories, Mexico, and Central

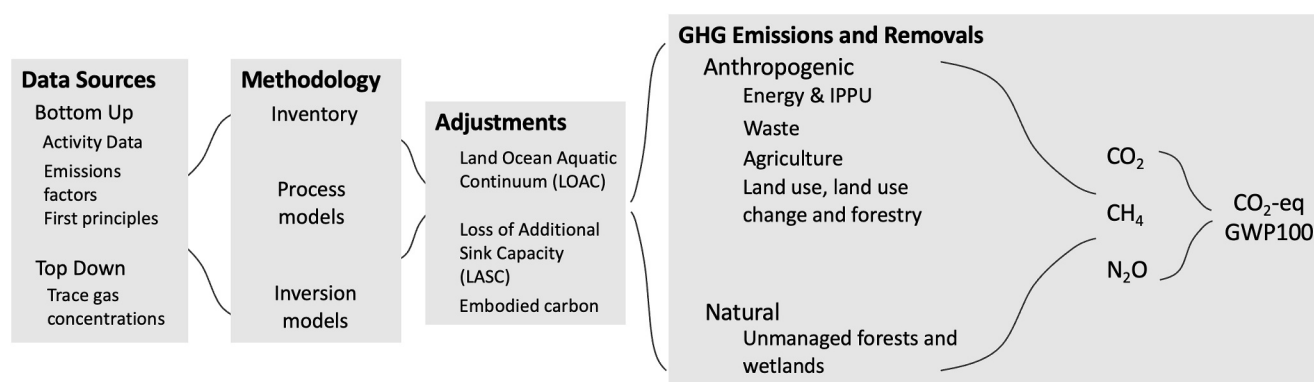


Figure 1. The workflow implemented in RECCAP2 to estimate net CO₂-eq (GWP100) emissions for North America and the four sub-regions for 2000–2009 and 2010–2019. RECCAP2 develops GHG budgets using data from inventories, process-based models (based on a first principles of biogeochemistry), and atmospheric inversions that are integrated and adjusted for lateral fluxes and differences in definitions and terminology.

America (including the Caribbean). Within these regions, the GHG budgets quantify fluxes for terrestrial, freshwater, nearshore-coastal ecosystems and the Exclusive Economic Zones (EEZ) in the case of continental shelf CO₂ exchange.

2.2. Overview

Data sets include direct atmospheric observations of trace gases, published emission factors, and satellite-based products for land cover, biomass, and column GHG concentrations. These data are used in a variety of modeling approaches that include bookkeeping models, data-driven models, process-based forward models, and atmospheric inversion models (Figure 1). These models provide emissions source and removal (sink) estimates for all anthropogenic and natural fluxes, and follow the definitions and sectors described by Ciais et al. (2022) for CO₂, and Saunio et al. (2020, 2024) for CH₄ and Tian et al. (2020, 2024) for N₂O. The GHG budget is presented for two decadal epochs, 2000–2009 and 2010–2019, using units expressed in Teragrams (1 Tg = 10¹² g) for CO₂, and CH₄, and gigagrams (1 Gg = 10⁹ g) for N₂O. The budget integration to CO₂-eq follows the Intergovernmental Panel on Climate Change (IPCC) Sixth Assessment Report's 100-year GWP to convert all anthropogenic and managed land GHG fluxes and stock changes to CO₂-equivalents (Forster et al., 2024).

2.3. Fossil and Cement Production Emissions for CO₂, CH₄, and N₂O

CO₂, CH₄ and N₂O emissions from fossil fuel activities, cement production and the burning of biomass and biofuel for energy were estimated from an ensemble of inventories. For CO₂, sources of emissions are from the combustion of coal, oil and gas (including flaring) and production of cement via clinker production (Friedlingstein et al., 2023). Bunker fuels, from fossil fuel combustion activities related to shipping and aviation, are included in a subset of the CO₂ inventories (i.e., the NIR and the Open-Source Data Inventory of Anthropogenic CO₂ (ODIAC)). The fossil CO₂ inventories do not include the cement carbonation sink (Friedlingstein et al., 2023). CH₄ fossil emissions sources are from activities related to coal, oil and gas exploitation, including flaring and liquified natural gas storage and transport (Saunio et al., 2020). N₂O emissions from industrial processes are mainly from the oxidization of nitrogen compounds during the production processes of both nitric and adipic acid, which are used for making synthetic fertilizers and synthetic fibers (Tian et al., 2024). Our fossil inventories combine emissions from energy production categories with those categories from Industrial Processes and Product Use (IPPU). The differences between the sources of the inventories stem mainly from uncertainties in the source of activity data and assumptions for emissions factors.

The specific inventories are described in more detail in Table S1 in Supporting Information S1, and they include the United Nations Framework Convention on Climate Change (UNFCCC) National Inventory Reports (NIR submitted in 2022, with end reporting year of 2020) and Biennial Update Reports (BUR), the Global Carbon Project's fossil CO₂ emissions data set (GCP2020), the International Energy Agency (IEA) Methane Tracker Database 2022, the International Institute for Applied Systems Analysis Greenhouse Gas and Air Pollution Interactions and Synergies (GAINS), the Global Fuel Exploitation Inventory (GFELv2), and priors used in the

Orbiting Carbon Observatory-2 Model Intercomparison (OCO2-MIP). Gridded products include the Global Carbon Project's Gridded Fossil Emissions Data set version 2020.1 (GridFED), the European Union's Joint Research Center's Emissions Data set for Global Atmospheric Research (EDGAR) v6.0, the Pacific Northwest National Laboratory's Community Emissions Data System (CEDS) and the Open-Source Data Inventory of Anthropogenic CO₂ (ODIAC2022), which uses nightlights to spatially disaggregate the Carbon Dioxide Information Analysis Center (CDIAC). National and city-scale inventories such as VULCAN (Gurney et al., 2020), HESTIA or the near real time CarbonMonitor data set (Liu et al., 2022) were not included due to the spatial or temporal domain not covering the full spatial and temporal domain of the North America RECCAP2.

The NIR, BUR, GCP2020, GAINS, and IEA inventories are provided at the national scale compared to spatially disaggregated data provided by GridFED, EDGAR v6.0, CEDS, GFEIv2, OCO2-MIP and ODIAC. The spatially disaggregated emissions data sets are also used as input to atmospheric inversions or forward models. IEA and GFEIv2 are available only for fossil CH₄ and the spatially explicit prior fossil CO₂ emission map used for OCO2-MIP is developed by hybridizing ODIAC2020 and CarbonMonitor. Bunker fuels, ~2.8% of total global emissions, are included separately in the NIR, ODIAC and CEDS emissions inventories. Non-territorial emissions (i.e., emissions of CO₂ from exported coal, oil and gas) and consumption emissions using data from the Global Trade Analysis Project (GTAP) (Peters et al., 2012) were used from Friedlingstein et al. (2023). The differences between fossil CO₂ emissions products were recently reviewed by Andrew (2020).

2.4. Waste Emissions (CO₂, CH₄, N₂O)

Waste emissions include emissions from organic solid waste contained in landfills, wastewater management, and biomass incineration that is not used in energy production (Table S2 in Supporting Information S1). Emissions for the three gases are reported to the UNFCCC in the NIR and BUR submissions, other estimates are provided for by EDGARv6, CEDS, and GAINS (only CH₄). The waste emissions estimates are derived from activity-based approaches and generally follow the IPCC (2006) guidelines using various assumptions for the application of emission factors.

2.5. Agriculture Emissions (CO₂, CH₄, N₂O)

Agriculture-related emissions include direct and indirect emissions associated mainly with crop and livestock production but also smaller sources from aquaculture in coastal wetlands. This includes direct CH₄ emissions from enteric fermentation from livestock, the management of manure, rice cultivation, liming and urea applications to soil (in the case of CO₂), and the emissions of N₂O from the application and conversion of synthetic or organic nitrogen fertilizers to soil N₂O emissions, agriculture waste burning and aquaculture. Indirect emissions of N₂O include those due to N deposition and leaching in aquatic systems. IPCC Guidelines (2006) include emissions from prescribed burning of savannas, but these were not recorded in any of the data sets that we used in this study. Data are provided by the UNFCCC NIR and BUR, EDGARv6, CEDS, GAINS (CH₄ only), see Table S3 in Supporting Information S1, and additional agriculture direct N₂O emissions data from land process models used in the Nitrogen Model Intercomparison Project 2 (NMIP2).

2.6. Top-Down Atmospheric Inversions (CO₂, CH₄, N₂O)

Atmospheric inversions provide a “top-down” constraint on the exchange of CO₂, CH₄ or N₂O between the land or ocean and atmosphere. Combining a priori estimates of anthropogenic and natural fluxes with 3-dimensional wind fields, atmospheric inversions optimize surface fluxes to constrained with observed atmospheric concentrations. The spatial grid resolution of atmospheric inversions, roughly 100–300 km, is limited by the available observation network and computational needs as well as the data required for the atmospheric transport simulation. The resulting posterior fluxes are then partitioned to biospheric fluxes for CO₂ (i.e., net-biome production (NBP) = $-1 \times \text{net ecosystem exchange (NEE)} - F_{\text{fire}}$), and fossil, wetland, non-wetland, agriculture/waste, and biofuel for CH₄, and only the total net flux for N₂O. The NBP estimated by atmospheric inversions includes all of the exchange of CO₂ between the land and atmosphere (and is thus more similar to Net Ecosystem Exchange, NEE), with contributions from weathering and geological emissions. The “top down” estimates however do not directly estimate carbon fluxes induced by lateral transport from trade and aquatic processes and estimates of which (as described below) are used to “correct” the atmospheric fluxes by adjusting for the lateral fluxes.

Inversions generally ignore contributions from reduced carbon compounds from biogenic volatile organic compounds (BVOC), carbon monoxide (CO) from fossil fuels and fire, and CH₄ emissions.

Data for the atmospheric CO₂ inversions were obtained from the Global Carbon Budget 2021 (Friedlingstein et al., 2023). The ensemble includes six inversion models (CAMS v20r2, Jena CarbonScope v2021, CarbonTracker Europe, NISMON-CO₂ v2021.1, University of Edinburgh, and CMS-Flux) covering the time period up to 2020 (Table S4 in Supporting Information S1). The CMS-Flux inversion uses the ACOS-GOSAT and OCO-2 b10 retrievals of XCO₂ whereas the other inversions use flask air samples and in situ data from ObsPack GLOB-ALVIEW+v6.1 (Masarie et al., 2014) and NRT_v6.1.1. The inversions all use GridFEDv2021.2 as a prior but differ in the priors used for the biosphere and ocean surface fluxes. The inversions also use different transport models and wind fields, with ERA used for TM3, TM5 and LMDZ v6, MERRA2 for GEOS-CHEM and JRA-55 for NICAM-TM, as well as different optimization approaches, that is, ensemble Kalman filter, conjugate gradient, or variational schemes. The posterior land-atmosphere fluxes (NBP) were adjusted to compare with bottom-up estimates by subtracting the cement carbonation sink, which is not accounted for in GridFEDv2020.1, and lateral transport by rivers.

The lateral transport of organic carbon by rivers (F_{ie} , total fluvial load minus amount of carbon derived from solution of lithospheric carbonates) was estimated by scaling GlobalNEWS2 (Mayorga et al., 2010) adjusted for lithogenic carbon (Ciais et al., 2022; Hartmann et al., 2009) to match the latitudinal patterns of Resplandy et al. (2018) and to a global export constraint of 500 TgC yr⁻¹ (Regnier et al., 2013). Globally, the total fluvial carbon load in lateral transport sums to 728 TgC or 2,669 4 TgCO₂ yr⁻¹ (Battin et al., 2023). In addition to the GCB ensemble, we use inversions from the v10 OCO2-MIP (Byrne et al., 2023) to develop a larger ensemble of satellite-based retrievals. OCO2-MIP includes 11 inversion systems using the same fossil fuel prior (ODI-AC2020+CarbonMonitor) with different transport models and biospheric and oceanic priors. We contrast the OCO2-MIP in situ and land-nadir-land-glint (LNLG) inversions for net biosphere exchange (where OCO2-MIP defines $NBE = -1 * NEE = F_{fire} + Reco - GPP$, including land management and lateral processes, and GPP is gross primary production), for net carbon exchange ($NCE = NBE + FF$) and for delta-carbon ($dC = NBE - F_{crop} - F_{wood} - F_{river}$) which removes from NBE all CO₂ fluxes that do not result in changes of land carbon storage in the region considered.

The atmospheric CH₄ inversions included five inversion systems using satellite CH₄ retrievals from GOSAT and nine inversion systems using in situ data from NOAA ObsPack, see Table S5 in Supporting Information S1. Priors were provided to the inversion modelers for fossil, agriculture and waste (EDGARv4.3.2), fire (GFED4.1s), wetlands (Poulter et al., 2017), and termites (Kirschke et al., 2013). The OH chemical sink was model dependent and prescribed (rather than interactive) using data from chemical transport models. Posterior CH₄ flux sectors include total emissions, the upland methanotrophy sink, net CH₄ emissions, fossil fuel, wetlands, non-wetlands, agriculture and waste, and biofuel.

For N₂O, the inversions were carried out using four inversion systems (PYVAR-CAMS, MICRO4-ACTM, INVICAT, and GEOS-Chem) as part of NMIP2 (Tian et al., 2024). In situ air samples were used from NOAA and other atmospheric sampling networks and surface priors for anthropogenic emissions were used from EDGARv4.2 (1997–2004) and EDGARv5 (2005–2020), and from biospheric and ocean models for agriculture and natural fluxes. The N₂O inversions used EDGVARv6 for fossil and waste N₂O, and different priors for agriculture, for example, OCN was used in TOMCAT, MIROC4 used VISIT, and GEOS-CHEM used EDGAR. The posterior flux was not partitioned to different sectors and so the inversion optimizes the total fossil, agricultural and natural N₂O emissions for all sectors combined.

2.7. Biospheric Carbon Exchange (CO₂)

We use the term biospheric carbon exchange to represent fluxes of CO₂ from terrestrial ecosystems that include managed and unmanaged components. We follow the approach of Chapin et al. (2006) and Ciais et al. (2022) in defining net ecosystem production (NEP) as $NEP = Ra + Rh - GPP$, and net biome production (NBP) as $dC = NBP = NEP - F_{fire} - F_{ie}$, where dC is change in carbon stocks. We use data from process-based models, data-driven approaches, and national GHG inventories to estimate NBP. Compared to the definition of NBP used for atmospheric inversions, process-model estimates of NBP do not include the land-atmosphere fluxes arising from lateral components from aquatic and trade fluxes or contributions from reduced carbon compounds and weathering. The main differences between the approaches are as follows. Process-based land models use “first

principles” to prognostically simulate gross primary production (F_{GPP}), autotrophic respiration (F_{Ra}) and heterotrophic respiration (F_{Rh}), and some combination of fire (F_{fire}), deforestation (D), wood and crop harvest (H), and product pools decomposition (P), but not the lateral exchanges of H and P. Remote sensing based products can predict NEE directly using flux towers as training data sets, that is, FluxCom (Tramontana et al., 2016). More recently, time series of gridded biomass retrievals made from Soil Moisture and Ocean Salinity (SMOS) using the vegetation optical depth (VOD, (Rodríguez-Fernández et al., 2018)) or directly from the brightness temperatures (Salazar-Neira et al., 2023) have been used to reconstruct NBP-like fluxes using a stock-change approach, for example, (Fan et al., 2019). The SMOS-based aboveground annual biomass change includes emissions and removals from land use change, disturbance, and lateral processes and is thus more representative of dC derived from atmospheric inversions, although it does not include carbon stock changes in litter and soils. We also use land carbon stock change data from the NIR Land Use, Land Use Change and Forestry sector (LULUCF), described below.

The TRENDYv9 (covering up to the year 2019) model ensemble from the Global Carbon Budget (Friedlingstein et al., 2020), was used to provide gridded NBP estimates. TRENDYv9 includes 19 dynamic global vegetation models (DGVM) forced by meteorology from CRUts4.04, land use and land cover change from the Land-Use Harmonization v2 (LUH2) data set (Chini et al., 2021), and annual atmospheric CO_2 concentrations provided by NOAA’s marine boundary layer network. The S3 scenario was used here, which includes simulations at 0.5-degree resolution forced with changing climate, CO_2 , and transient land-use change for the period 1700–2019. Nine of the (19) models included interactive fire modules, and land-use change was represented with different levels of complexity with respect to shifting cultivation, wood harvest and inclusion of product pools. Some of the key differences in land-use change modules include the treatment of prescribing crop types versus generalized pasture or rangeland grasses, the implementation of crop and wood harvesting and treatment of emissions from residue and product pools (Friedlingstein et al., 2020). The land-use change carbon fluxes from TRENDY models include the foregone sink over natural land replaced by cultivated land or secondary forest (called “Loss of Additional Sink Capacity (LASC)” and explained in next section).

We use FluxCom to provide a data-driven estimate for NEE. FluxCom applies machine learning algorithms to train an ensemble of models using eddy covariance observations and predictor data from meteorology (ERA5) and surface reflectance (Tramontana et al., 2016). Two monthly products were assessed, both at 1-km resolution, with one using remote sensing reflectance only (RS) and another using RS and meteorology combined. Because FluxCom is trained on towers that are generally protected from land use change and wildfire, these fluxes are not included as losses in the upscaled product.

We also use multiangular L-band brightness temperatures (TBs) to derive NBP based on the carbon-stock change approach (Salazar-Neira et al., 2023). The L-band passive microwave retrievals are derived from the SMOS mission and biomass is estimated using the L-band Vegetation Optical Depth and a parametric approach (PARAM) or directly from the L-band TBs using an artificial neural network (ANN). In both cases, the relationship to estimate biomass was obtained using as reference the European Space Agency’s Climate Change Initiative (CCI) Biomass product (Santoro et al., 2021). NBP is then calculated annually by subtracting the previous year biomass estimate from current year.

NBP is also estimated from the nationally submitted NIR and BURs following the approach of Deng et al. (2022). The total LULUCF is estimated as the net emissions and removals from land cover types remaining in their original state and also the conversion across the full matrix of land cover transitions. In addition, harvested wood products (HWP) are also included in LULUCF. The countries use different approaches to estimate emissions and removals, with the Carbon Budget Model of the Canadian Forest Sector (CBM-CFS) used in Canada (Kurz et al., 2018), the US Forest Inventory and Analysis plots used in the USA, and a version of the CBM forestry model used in Mexico. The inventories treat disturbances differently, with the sample plots inherently including natural and anthropogenic disturbances for the USA and Mexico inventories, and large-scale (wildfire) disturbances generally excluded from the gain-loss approach used in the Canadian inventory (Harris et al., 2016). For croplands, we use an estimate of NEE from Hayes et al. (2012), which was estimated from data on cropland soil carbon change and heterotrophic respiration losses for different crop types and soil management systems.

Lastly, we also include the net CO_2 fluxes from the World Resources Institute carbon flux (WRIcf) model (Harris et al., 2021) and FAOSTAT (Tubiello et al., 2021). The WRIcf model uses a forest gain-loss approach that combines remotely sensed biomass data from circa 2000 with the forest-gain and forest loss product of Hansen

et al. (2013). Emissions are estimated as forest is lost to non-forest, and removals are estimated following IPCC (2006, 2019) guidelines through the use of standardized forest regrowth curves. The data are provided as the average for 2000–2020. The FAOSTAT-derived emissions data come from the forest land emissions data set (element/item code 72332/6751) and the “forestland” category, that is, forest-to-forest change, that estimates stock changes based on a gain-loss approach.

2.8. Land Use and Land-Cover Change Fluxes

Fluxes from land-use and land-cover change include losses of carbon from deforestation, shifting cultivation, forest degradation, wood and crop harvest, grazing, peat fires and drainage, soil carbon losses, and atmospheric removals from gains in carbon due to forest regrowth. In addition to the numerous processes contributing to LULUCF emissions, varying assumptions exist with respect to the treatment of legacy emissions, committed emissions, product pools and the transient effects of climate and CO₂ on biomass change. Here we compile LULUCF emissions from inventories (NIR, BUR, and FAOSTAT), and the bookkeeping models OSCAR (Gasser et al., 2020), Houghton and Nassikas (2017) (H&N; 2017) and BLUE (Hansis et al., 2015) and process models (TRENDYv9, (Sitch et al., 2015)). We develop adjustment terms, that is, the loss of additional sink capacity (LASC; described below), and follow the approach of Grassi et al. (2023) and Friedlingstein et al. (2023) to reconcile the estimates (Table S6 in Supporting Information S1).

The national inventory reports (i.e., NIR and BUR) provide emissions and removals for the transitions between the full matrix of the five IPCC land cover categories (forests, settlements, croplands, wetlands, and grasslands). The primary data source for the USA is the FIA database. For Canada the Canadian Forest Inventory (CanFI) and the carbon fluxes are tracked for biomass, dead organic matter and soil mineral carbon using IPCC emission factors. Following Grassi et al. (2023), we estimate LULUCF emissions as the integration of emissions and removals over all land-use transitions, including HWPs, and estimate deforestation fluxes for forest conversion to other IPCC land use categories, both using data from the CRF. For FAOSTAT, the database provides country-level LULUCF estimates using a global Tier 1 approach to estimate emissions and removals using element/item code 72332/6750 for net-forest conversion (Tubiello et al., 2021). Forest area for FAOSTAT is used from the Forest Resource Assessment (FRA) and combined with emission factors provided by IPCC (2006).

The bookkeeping models (BMs) do not use inventory data or follow the IPCC land cover categories and instead use changes in forest area data from FAOSTAT in the case of H&N, LUH2 for BLUE, and both LUH2 and FAO for OSCAR. Each year, the BMs track changes in forest area and the time since regrowth and use forest growth and decay curves with predefined stocks to estimate emissions and removals. The models also include carbon emissions from peatland drainage and degradation using fire data from the Global Fire Emissions Database (GFED4s) and drainage data from FAO (Conchedda & Tubiello, 2020). BLUE and H&N exclude any response of stocks and growth curves to climate and CO₂ fertilization, instead using fixed carbon densities over time. The OSCAR bookkeeping model includes a transient biomass response and is thus able to track land-use emissions as well as account for the effect of the reference year for no land cover change (typically 1860). The use of the reference simulation and transient land-cover simulation to estimate emissions leads to inflated emission estimates because of how CO₂ fertilization leads to more greater carbon storage in the reference simulation, which has higher forest area. This effect is known as the loss of additional sink capacity (Pongratz et al., 2021) and can account for around 40% of emissions.

LULUCF emissions were estimated from the TRENDYv9 ensemble as the difference between a simulation that held land cover constant for year 1860 (S2 scenario) and the S3 scenario described previously. The same driver data used to estimate NBP were used in both scenarios (CRU, LUH2, and transient atmospheric CO₂). Differencing the two scenarios provides an LULUCF estimate that includes legacy fluxes from soils, regrowth of forests, as well the cumulative loss of additional sink capacity term (LASC). The LASC term means that the LULUCF emissions are larger because the cumulative CO₂ fertilization effect on the S2 scenario (with a fixed 1860 land cover for the full simulation) is more significant due to the presence of greater forest area with longer carbon turnover times. We therefore diagnose the magnitude of the LASC term following Obermeier et al. (2021) for the TRENDYv7 ensemble that provided additional simulations referred to as S5 (fixed present-day climate and CO₂, transient land use) and S6 (fixed present-day climate and CO₂, pre-industrial land use). The combination of S2, S3, S5, and S6 simulations is used to estimate the “present-day versus transient differences (PTD)” environmental conditions difference (PTD) as $PTD = F_{LULCC_pd} - F_{LULCC_trans} = (NBP_{S6} - NBP_{S5}) - (NBP_{S2} - NBP_{S3})$.

2.9. Vegetated Freshwater Wetland Emissions (CH₄)

Wetland ecosystems produce CH₄ as a by-product of anaerobic decomposition due to the presence of methanogenic bacteria in oxygen-deprived, flooded soils. For vegetated freshwater wetlands, including swamps, bogs and fens, we use data from the Global Methane Budget (GMB) wetland model ensemble (Zhang et al., 2024) and data from the UpCH₄ database (McNicol et al., 2023). While the NIRs report wetland CH₄ emissions from “flooded land remaining flooded lands” and “coastal wetlands,” these emissions are only for managed wetlands and thus we do not include these in natural wetlands assessment. The GMB ensemble includes 13 land-surface models that simulate CH₄ emissions as a function of soil carbon, soil moisture and soil temperature, using a diagnostic wetland scheme to predict the presence and temporal dynamics of wetlands. The diagnostic wetlands come from a hybrid remote-sensing wetland inventory data set called the Wetland Area Dynamics for Methane Modeling (WAD2M) data set (Zhang et al., 2021) and the wetland models use meteorology data from the Climate Research Unit (CRU)-Japanese Reanalysis (JRA) and observed annual atmospheric CO₂ concentrations. The UpCH₄ data set uses a global network of 43 eddy-covariance sites, Fluxnet-CH₄ (Knox et al., 2019), to train a machine-learning based approach using a set of 140 candidate environmental predictors with CH₄ fluxes.

2.10. Land Ocean Aquatic Continuum (LOAC) Fluxes

GHG flux data across the land-ocean aquatic continuum (LOAC) were provided by three RECCAP2 LOAC synthesis studies, recent literature, and SOCCR2 outputs (Table S7 in Supporting Information S1). New data on the export of carbon from inland waters to estuary fluxes (F_{ie}) were calculated by the RECCAP2 LOAC Group I for total carbon (TC), particulate organic carbon (POC), particulate inorganic carbon (PIC), dissolved organic carbon (DOC), dissolved inorganic carbon (DIC) (Liu et al., 2024). Outgassing and evasive fluxes for inland waters, including rivers, streams, lakes, ponds, and reservoirs, were estimated for North America as a whole by LOAC Group II (Lauerwald et al., 2023a, 2023b) and for the North American sub-regions using gridded data as described below. Evasive and (carbon) burial fluxes for estuaries and coastal vegetation were estimated by LOAC Group III (Rosentreter et al., 2023). Additional data for river and lake carbon burial rates, CO₂ sea-air exchange, and continental shelf carbon burial rates were used from SOCCR2 (Butman et al., 2018; Fennel et al., 2018).

Carbon export from inland waters to estuaries (F_{ie}) of TC, DOC, DIC, and POC and PIC, were estimated from an ensemble compilation of published data and study-specific regression-based approaches (Liu et al., 2024). The Liu et al. (2024) data product generated LOAC estimates for each of the ~5,500 river basins demarcated within the University of New Hampshire Global Hydrological Archive and Analysis System model (UNH-GHAAS; (Vörösmarty et al., 2000)). In cases where river basins spanned international boundaries within North America, lateral flux estimates were divided between countries (including Greenland) using calculated estimates of the proportional geographic coverage of watersheds in each country. Lateral fluxes of DIC were partitioned into fractions derived from atmospheric CO₂ fixation and those derived from rock dissolution, based on mostly United States-specific estimates by Moosdorf et al. (2011) with acknowledgment that this generalization may result in bias for Mexico and Central America. These F_{ie} lateral fluxes represent the movement of carbon from the point of freshwater outflow to the coastal margin. DOC and POC include the F_{ie} lateral fluxes of organic carbon derived from soil leachate, erosion, and primary production within the aquatic continuum, PIC is generally derived from erosion of rock, and DIC is derived from dissolution of carbonate rocks (i.e., silicate rock weathering, $\text{CaSiO}_3 + 2\text{CO}_2 + \text{H}_2\text{O} \rightarrow \text{Ca}^{2+} + 2\text{HCO}_3^- + \text{SiO}_{-2}$) and fixation of CO₂ as bicarbonate during chemical weathering (i.e., carbonate rock weathering, $\text{CaMg}(\text{CO}_3)_2 + 2\text{CO}_2 + 2\text{H}_2\text{O} \rightarrow \text{Ca}^{2+} + \text{Mg}^{2+} + 4\text{HCO}_3^-$). Over decadal to centennial timescales, we ignored additional processes that return some of the DIC from carbonate rock weathering back to the atmosphere over much longer time scales. Weathering uptake of atmospheric CO₂ was derived from estimates made by Hartmann et al. (2009). These data represent the total mobilization of dissolved inorganic carbon from weathering and the weathering CO₂ sink. The “DICatm” term is the part of the DIC that provides CO₂ sequestered in the weathering process. DIC minus DIC atm provides the part of DIC that results from dissolved carbonate minerals.

For outgassing and evasive fluxes from rivers and lakes (F_{ia}) at the sub-region level, we used gridded data products that were suitable for partitioning; as a result, these outputs use only a subset of the LOAC group II ensemble estimates (Lauerwald et al., 2023a, 2023b). For sub-regional CO₂ emissions from lakes we used the data sets of Raymond et al. (2013) as gridded by Zscheischler et al. (2017), and for rivers we used data from Liu, Kuhn, et al. (2022) and Liu, Deng, et al. (2022). For regional lake and river emissions, we used data from the review of

Lauerwald et al., 2023b). For CH_4 emissions from lakes, we used the estimate of Stavert et al. (2022). For CH_4 emissions from rivers and streams, we used the gridded product in Rocher-Ros et al. (2023). For N_2O emissions from lakes and rivers, we used Lauerwald et al. (2019) and Maavara et al. (2019), respectively. Where they were available separately, we provide compiled emissions from lake classes 1 (natural lakes), 2 (reservoirs), and 3 (lakes regulated by a dam), as defined in the HydroLAKES database (Messenger et al., 2016). For N_2O emissions, we included denitrification processes as outlined in Lauerwald et al. (2019) and Maavara et al. (2019), which also includes nitrification.

Estuarine (tidal systems and deltas, lagoons, and fjords) and coastal (mangroves, salt marshes, seagrasses) fluxes were provided by LOAC Group III (Rosentreter et al., 2023). These systems include oligohaline, mesohaline and polyhaline coastal ecosystems with a salinity >0.5 ppt, thus excluding freshwater systems. Surface areas for each estuarine or coastal system were stratified by RECCAP2 region and sub-regions using the MARGins and CATchments Segmentation database of Laruelle et al. (2013) for estuaries, Global Mangrove Watch (Bunting et al., 2018), the global map of salt marshes (Mcowen et al., 2017) and the United Nations Environment Program's seagrasses map (UNEP-WCMC & Short, 2005) combined with SOCCR2 estimates for coastal system surface areas. GHG emissions were estimated by combining the area of each system with the average flux rate for each of the three gases to estimate (a) water-to-air estuarine GHG fluxes (F_{ea}), (b) coastal NEE (F_{aw}), (c) estuarine organic carbon burial rates ($F_{\text{ws+es}}$), (d) coastal margin inputs (i.e., lateral flux from land to ocean from organic and inorganic submarine groundwater discharge) and (e) riverine input to the ocean. The latter two fluxes determine the ocean carbon residence time under steady-state assumptions, which is partly an indicator of the efficiency of lateral carbon inputs related to ocean CO_2 removal.

To complete the LOAC budgets, we used estimates for continental shelf air-sea exchange (F_{ac}) from Resplandy et al. (2024), and lake and river burial (F_{ls}) and continental shelf burial rates (F_{cs}) from SOCCR2 (Butman et al., 2018; Fennel et al., 2018). F_{ac} was estimated as the mean of four observation based pCO_2 products from Carboscope, CMEMS, Coastal-SOM-FFN and Merged-SOM-FFN. The continental shelf regions for Canada, the USA, Mexico, and CA + CAR were matched with the sub-regions from Figure 16.1 in Fennel et al. (2018) and the values in Table 16.4 used to estimate F_{cs} . The F_{cs} flux was then area-weighted and reduced by 78% to match the smaller continental-shelf area used by Resplandy et al. (2024) to estimate F_{ac} (5.1 Mkm^2 compared to 22.99 Mkm^2 used in SOCCR2 (Fennel et al., 2018)). The F_{cs} and F_{ac} terms are not included in the bottom up estimate of the net territorial flux (Equation 1) and the terms are estimated only to complete the LOAC components. The lateral flux from land to inland waters (F_{li}) was thus computed as $F_{\text{ie}} + F_{\text{ia}} + F_{\text{is}}$, the export to estuaries (F_{ec}) is estimated as $F_{\text{ie}} - F_{\text{es}} - F_{\text{ea}} - F_{\text{aw}}$ and the lateral export from continental shelf to open ocean (F_{co}) as $F_{\text{ec}} - F_{\text{cs}} + F_{\text{ac}}$ following Regnier et al. (2022).

2.11. Crop and Wood Trade Fluxes

Lateral fluxes of carbon embodied in trade products are an important component for reconciling top-down and bottom-up approaches. To estimate crop lateral fluxes, we used FAOSTAT data to calculate crop and wood harvest for each sub-region and included FAOSTAT adjustments to account for crop import and export. For wood products, we used FAOSTAT wood harvest data and FAOSTAT import and export statistics to estimate changes in carbon pools using the Wood Products Carbon Storage Estimator (WPSCS Estimator) (Wei et al., 2023). We compared our estimates with OCO2-MIP net crop and wood trade statistics (Byrne et al., 2023) and to the National Inventory Reports for Mexico, USA and Canada, and SOCCR2 (Birdsey et al., 2018; Domke et al., 2024; Hristov et al., 2018).

The FAOSTAT "primary" crop production statistics (element code 5510) are provided annually for harvested crops (~ 119 for CA + CAR, 112 for Mexico, 94 for USA and 62 for Canada). We aggregated the data by sub-region and converted from tonnes of dry matter (assumed for all crops) to TgCO_2 assuming 50% carbon content and using the molecular ratio of CO_2 to C. Annual FAOSTAT crop import and export statistics were used to estimate the total crop consumption as $C_{\text{cons}} = \text{production} + (\text{import} - \text{export})$. To estimate human crop consumption emissions (H_{e}), we used the model of West et al. (2009) that assumes a per capita consumption rate of 54 kgC yr^{-1} and combined this with annual FAOSTAT human population data. Livestock consumption (L_{e}) emissions were estimated as $C_{\text{cons}} - H_{\text{e}} - E$, where E is an adjustment for carbon lost via enteric CH_4 emissions using NIR data following Hayes et al. (2012).

Total wood consumption was estimated as $W_{\text{cons}} = W_{\text{harvest}} + (W_{\text{import}} - W_{\text{export}})$ using annual harvest statistics from FAOSTAT for Canada, Mexico, Central America and Caribbean, and EPA NGHGI data for the USA. Import and export statistics were used from the World Integrated Trade Solution (WITS) database. The wood products include primary wood products such as roundwood, sawlogs and veneer logs, pulpwood and particle board and are converted to carbon following Ciais et al. (2021). The emissions for wood harvested for fuel use would be included in the NIR Harvested Wood Pool category and we do not track these here. The WPsCS estimator was used to compute wood product use (firewood or product use), end-use pool size, landfill pools, and landfill emissions of CO₂ assuming different life cycles for paper, landfill, furniture, and construction materials. Two different assumptions were made to estimate import and export given the extensive internal trade among North American countries and to avoid double counting (see Supporting Information S1). For example, 90% of Canada's wood product exports are destined for other North American countries and would show up as an import to the North American budget if not accounted for.

2.12. Other GHG Fluxes and Stocks

Other biogenic fluxes (and stocks for carbon) and geologic fluxes of the three GHG's were summarized to help provide components of the budgets and to help contextualize fluxes with stock change information. Gross primary production (GPP) data were simulated by the process-based global vegetation models (TRENDYv9 S3) and remote-sensing (RS) data-driven models such as FluxSat (Joiner & Yoshida, 2020), FluxCom (one version using ERA5 meteorology and another with only RS input data), and GOSIF (Li & Xiao, 2019). Net primary production was simulated by the same set of forward models and also using the MODIS (MOD17) NPP algorithm (Zhao et al., 2005). Heterotrophic respiration (Rh) was also provided by the forward models, as well as from FluxCom (ERA5 and RS), and the "global soil respiration database (SRDB)" (Stell et al., 2021). Wildfire emissions were estimated by the same set of forward models from TRENDYv9 (CO₂ only), and from remote-sensing driven models, including GFEDv4.1s for CO₂, CH₄, N₂O, and CO (van der Werf et al., 2010), and the Quick Fire Emissions Database (QFED) for CO₂. The NIR provided wildfire CO₂ emissions for Canada, and CH₄ and N₂O wildfire emissions for USA and Canada, but not Mexico. Insect-related CO₂ emissions were provided in the Canadian inventory.

We used emissions data for biogenic volatile organic compounds (BVOC) from the Copernicus Atmospheric Monitoring System (CAMS-GLOB-BIOv1.2), which uses the Model of Emission of Gases and Aerosols from Nature (MEGANv2.1) driven by meteorological reanalysis of the European Center for Medium-Range Weather Forecasts (Guenther et al., 2012; Sindelarova et al., 2022). The database includes monthly emissions for 26 BVOCs (isoprene, monoterpenes, and associated compounds), which were aggregated to annual sums and converted from carbon to CO₂. We excluded the secondary effect of BVOCs on carbon monoxide production.

Carbon stock estimates were compiled for above and belowground biomass and for litter and soil. For biomass, estimates were used from the TRENDYv9 model ensemble, from NASA Global Ecosystem Dynamics Investigation (GEDI) Level 4 gridded biomass, the European Space Agency's Climate Change Initiative (ESA CCI 2018), ICESAT-2 and FAOSTAT (element code 72151). The first of these aboveground biomass data sets were evaluated by Hunka et al. (2023), who describe how estimation algorithms, instrument types (lidar vs. radar) and uncertainty assessment frameworks affect comparisons across products. Litter biomass was estimated using the TRENDYv9 ensemble, where litter biomass represents the balance between influx from leaf and woody biomass turnover and turnover to soil carbon pools and respiration losses. Soil carbon was estimated from the TRENDYv9 model ensemble and from the ISRIC World Soils Information SoilGrids v2.0 database (Poggio et al., 2021).

Geologic seepage estimates for CH₄ were used from the gridded database of Etiope et al. (2019) and from Möner and Etiope (2002). The seepage emissions include sources from volcanoes, mud volcanoes, geothermal sources, seeps, and micro-seepage. We removed marine coastal seepage of CH₄. Geogenic CO₂ emissions, that is, from geothermal and volcanic areas, that is, high-temperature fluid-rock interactions, crustal magma, and mantle degassing, were not included due to lack of data.

Given uncertainties relative to overall budget, we do not include termite CH₄ emissions, which globally account for $14.8 \pm 6.7 \text{ TgCH}_4 \text{ yr}^{-1}$, and for North America $\sim 1.2 \text{ TgCH}_4 \text{ yr}^{-1}$ (Ito, 2023).

2.13. GHG Wiring Diagram Components

The emissions and removals for each of the three GHGs are integrated using the approach of Ciais et al. (2022) for CO₂, Saunio et al. (2024) for CH₄, and Tian et al. (2024) for N₂O. These approaches combine the fluxes estimated by the bottom-up methodologies to calculate the net emissions. The top-down and bottom-up estimates for atmospheric growth are then compared with one another to assess uncertainties.

For CO₂ the individual component fluxes are integrated to balance the vertical and lateral exchanges of carbon between geologic, aquatic, terrestrial, and product pools. Thus, the net exchange of CO₂ between the surface and the atmosphere represents the regional contribution to the change in atmospheric carbon pools (dCO_2atm) for territorial and non-territorial emissions.

$$dCO_2atm_{territorial} = F_{ff-territorial} + (F_{RH} + F_{NPP}) + F_{fire} + F_{LUC} + F_{ag} + F_{waste} + F_{wooddecay} + F_{woodburning} + F_{weathering} + F_{lakes} + F_{rivers} + F_{estuaries} + F_{coastal} \quad (1)$$

$$dCO_2atm_{non-territorial} = dCO_2atm_{territorial} + F_{ff-non-territorial} + F_{wood} + F_{crop} \quad (2)$$

Where $F_{ff-territorial}$ is from the NIR, $F_{ff-non-territorial}$ is from GCB, F_{RH} , F_{NPP} , F_{fire} , and F_{LUC} are from TRENDY v9, F_{ag} and F_{waste} are from the NIR, $F_{wooddecay}$ and $F_{woodburning}$ are from WPCsCS, $F_{weathering}$ is from Hartmann et al. (2009), F_{lakes} and F_{rivers} from LOAC I, $F_{estuaries}$, $F_{coastal}$ are from LOAC II, and F_{wood} and F_{crop} represent the net (i.e., imports minus exports) of carbon transferred in (territorial) or out (non-territorial) as a result of the trade of wood and crop products, respectively, as calculated from FAOSTAT data.

The change in atmospheric CH₄, dCH_4atm , was estimated as:

$$dCH_4atm = (Wetlands_{Coastal} + Wetlands_{Estuaries} + Wetlands_{Rivers} + Wetlands_{Lakes} + Wetlands_{Veg}) + (Agriculture_{Rice} + Agriculture_{Enteric} + Agriculture_{Manure}) + Waste + (Fire_{Wildfire} + Fire_{Bioenergy}) + Fossil + Geologic - Sink_{Methanotrophy} \quad (3)$$

Where $Wetlands_{Coastal}$, $Wetlands_{Estuaries}$, $Wetlands_{Rivers}$, $Wetlands_{Lakes}$, $Wetlands_{Veg}$ are from LOAC I, II and the GMB models, $Agriculture_{Rice}$, $Agriculture_{Enteric}$, $Agriculture_{Manure}$ and $Waste$ are from the NIR, $Fire_{Wildfire}$, $Fire_{Bioenergy}$ from GFED and NIR, $Fossil$ from NIR, $Geologic$ from Etiope et al. (2019), and $Sink_{Methanotrophy}$ from inversions.

The change in atmospheric N₂O, dN_2Oatm , was estimated as:

$$dN_2Oatm = (Wetlands_{Coastal} + Wetlands_{Estuaries} + Wetlands_{Rivers} + Wetlands_{Lakes}) + (Agriculture_{Rice} + Agriculture_{Manure}) + Waste + Fire_{Wildfire} + Fossil \quad (4)$$

Where $Wetlands_{Coastal}$, $Wetlands_{Estuaries}$, $Wetlands_{Rivers}$, $Wetlands_{Lakes}$ are from LOAC I and II, $Agriculture_{Rice}$, $Agriculture_{Manure}$ and $Waste$ is from NIR, $Fire_{Wildfire}$ from GFED, and $Fossil$ is from the NIR or BUR.

2.14. Global Warming Potentials

The IPCC Sixth Assessment Report global warming potentials over 20-year and 100-year horizons. Here, we report GPW at 100-year horizon. For CH₄ (27 kgCO₂ per kgCH₄) and N₂O (273 kgCO₂ per kgN₂O) from Working Group I, Table 7.15 are used to estimate the CO₂-equivalent budget (CO₂-eq). We estimate the BU GWP budget using the approach described in the previous section to define dCO_2atm_{BU} , dCH_4atm_{BU} and dN_2Oatm_{BU} .

$$GWP_{BU} = dCO_2atm_{BU} + dCH_4atm_{BU} * 27 + dN_2Oatm_{BU} * 273 \quad (5)$$

We also provide a TD GWP estimate.

$$GWP_{TD} = dCO_2atm_{TD} + dCH_4atm_{TD} * 27 + dN_2Oatm_{TD} * 273 \quad (6)$$

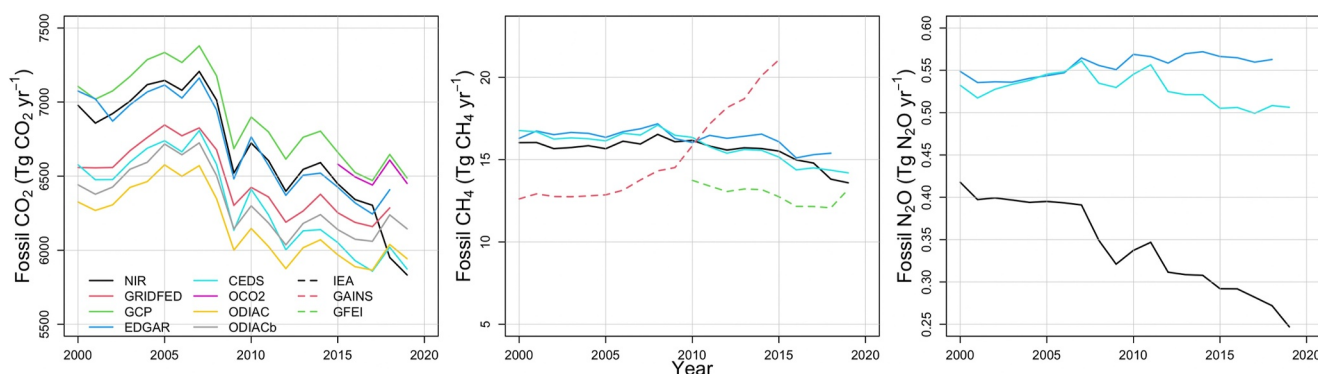


Figure 2. Total North American fossil fuel emissions CO_2 , CH_4 , and N_2O . The emissions include both direct emissions from combustion of coal, oil, gas, as well as indirect emissions of CH_4 from fossil fuel-related activities, and direct emissions of N_2O from industrial activities.

Where $\text{dCO}_{2\text{atm-TD}}$ is based on the GCB CO_2 inversions for natural sink and average of NIR, EDGAR, CEDS, GRIDFED and ODIAC fossil priors. The $\text{dCH}_{4\text{atm-TD}}$ the net emissions (sources minus sink) for the GMB wetland inversion ensemble and is $\text{dN}_{2\text{Oatm-TD}}$ is the net emissions from the NMIP model ensemble. The spread of the ensembles is used to provide an estimate of uncertainty.

3. Results

3.1. Fossil Fuel and Cement Carbon Emissions

North American territorial fossil fuel emissions for 2010–2019 averaged $6,398 \pm 225 \text{ TgCO}_2 \text{ yr}^{-1}$, $16.8 \pm 3 \text{ TgCH}_4 \text{ yr}^{-1}$, and $0.5 \pm 0.1 \text{ TgN}_2\text{O} \text{ yr}^{-1}$. Compared to 2000–2009 (Figure 2), fossil CO_2 emissions were lower (2000–2009: $6,851 \pm 227 \text{ TgCO}_2 \text{ yr}^{-1}$) but increased for CH_4 (2000–2009: $15.4 \pm 1 \text{ TgCH}_4 \text{ yr}^{-1}$) and were roughly the same for N_2O (2000–2009: $0.5 \pm 0.1 \text{ TgN}_2\text{O} \text{ yr}^{-1}$). Between 2010 and 2019, the USA was the largest North American emitter of CO_2 (Figure 3, $5,207 \pm 218 \text{ TgCO}_2 \text{ yr}^{-1}$), CH_4 ($12.9 \pm 2.9 \text{ TgCH}_4 \text{ yr}^{-1}$) and N_2O ($0.26 \pm 0.01 \text{ TgN}_2\text{O} \text{ yr}^{-1}$). Non-territorial regional emissions were $459 \text{ TgCO}_2 \text{ yr}^{-1}$ in 2000–2009 and decreased to $394 \text{ TgCO}_2 \text{ yr}^{-1}$ between 2010 and 2019. Regional bunker fuel emissions increased from $133 \text{ TgCO}_2 \text{ yr}^{-1}$ in 2000–2009 to $175 \text{ TgCO}_2 \text{ yr}^{-1}$ in 2010–2019. Regional consumption emissions decreased from $506 \text{ TgCO}_2 \text{ yr}^{-1}$ in 2000–2009 to $382 \text{ TgCO}_2 \text{ yr}^{-1}$ in 2010–2019. The largest uncertainties were for Mexico's N_2O emissions, which ranged from $0.017 \text{ TgN}_2\text{O} \text{ yr}^{-1}$ in the BUR to $0.25 \text{ TgN}_2\text{O} \text{ yr}^{-1}$ in EDGAR and CEDS.

3.2. Waste

Regional waste GHG emissions for 2000–2009 were $2.1 \pm 2.6 \text{ TgCO}_2 \text{ yr}^{-1}$, $9.3 \pm 0.8 \text{ TgCH}_4 \text{ yr}^{-1}$, and $0.05 \pm 0.03 \text{ TgN}_2\text{O} \text{ yr}^{-1}$ and for 2010–2019, $1.9 \pm 2.0 \text{ TgCO}_2 \text{ yr}^{-1}$, $8.9 \pm 0.9 \text{ TgCH}_4 \text{ yr}^{-1}$, and $0.06 \pm 0.03 \text{ TgN}_2\text{O} \text{ yr}^{-1}$. Uncertainties in waste CO_2 emissions were due to differences in how the USA NIR reported incineration of waste, with CO_2 as a by-product, within the “energy” sector and CEDS reported waste incineration CO_2 emissions in the “waste” sector. Waste CH_4 emissions (2010–2019) were highest in the USA ($5.5 \pm 0.8 \text{ TgCH}_4 \text{ yr}^{-1}$), followed by Mexico ($1.9 \pm 0.5 \text{ TgCH}_4 \text{ yr}^{-1}$), Canada ($0.9 \pm 0.1 \text{ TgCH}_4 \text{ yr}^{-1}$), and CA + CAR ($0.8 \pm 0.5 \text{ TgCH}_4 \text{ yr}^{-1}$), see Figure 3.

3.3. Agriculture

For 2010–2019, regional agriculture GHG emissions were $8.8 \pm 8.0 \text{ TgCO}_2 \text{ yr}^{-1}$, $13.5 \pm 1.9 \text{ TgCH}_4 \text{ yr}^{-1}$, and $1.2 \pm 0.3 \text{ TgN}_2\text{O} \text{ yr}^{-1}$ and for 2000–2009 were $7.6 \pm 6.9 \text{ TgCO}_2 \text{ yr}^{-1}$, $13.2 \pm 1.7 \text{ TgCH}_4 \text{ yr}^{-1}$, and $1.2 \pm 0.3 \text{ TgN}_2\text{O} \text{ yr}^{-1}$ (see Figure 4 for agriculture N_2O). The large uncertainties for CO_2 emissions were due to CEDS not including indirect- CO_2 emissions in their inventory for soil liming and urea application. Agriculture emissions were mainly from enteric fermentation processes, yielding $9.6 \text{ TgCH}_4 \text{ yr}^{-1}$ followed by manure management $2.7 \text{ TgCH}_4 \text{ yr}^{-1}$ and rice cultivation ($0.7 \text{ TgCH}_4 \text{ yr}^{-1}$). Rice cultivation, manure management, and enteric fermentation emissions were highest in the USA, 0.7 , 2.2 , $6.8 \text{ TgCH}_4 \text{ yr}^{-1}$. Mexico's total agriculture N_2O emissions were reported as $0.13 \text{ Tg N}_2\text{O} \text{ yr}^{-1}$ and only from manure management N_2O emissions.

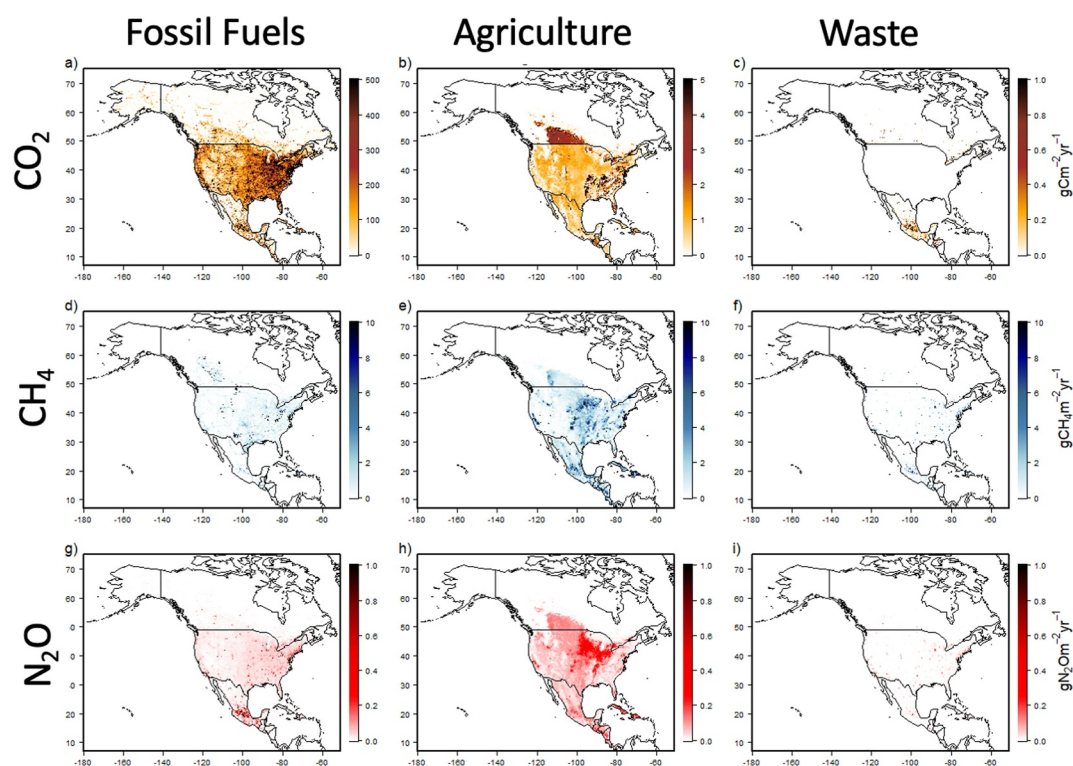


Figure 3. Spatial distribution of the annual anthropogenic GHG emissions for fossil fuels (left column), agriculture (middle column) and waste (right column). Data are gridded from the EDGAR v6 inventory for CO₂ (a–c), CH₄ (d–f), and N₂O (g–i).

3.4. Top-Down Budgets

For North America, the mean land-atmosphere flux (excluding fossil CO₂ emissions) for 2010–2019 using the Global Carbon Budget (GCB) inversions from Friedlingstein et al. (2023), was $-2,471.6 \pm 2,942.7$ TgCO₂ yr⁻¹ and the laterally adjusted flux was $-2,341 \pm 3,060$ TgCO₂ yr⁻¹. This means that the land-atmosphere CO₂ flux increased from 2000 to 2009 $-1,919.9 \pm 2,949.3$ TgCO₂ yr⁻¹, that is, sink became stronger. Compared with OCO2-MIP (LNLG: $-2,730 \pm 1,635$ TgCO₂ yr⁻¹, IS: $-3,154 \pm 1,992$ TgCO₂ yr⁻¹), the GCB CO₂ inversions were within the range of satellite-based retrievals.

For CH₄ inversions, the regional land to atmosphere flux (2010–2019) was estimated as 65.9 ± 15.5 TgCH₄ yr⁻¹, with the USA the highest emitter 39.8 ± 8.9 TgCH₄ yr⁻¹, followed by Canada 18.0 ± 4.4 TgCH₄ yr⁻¹. Net CH₄ emissions were estimated as 59.7 ± 15.3 TgCH₄ yr⁻¹, with 12.9 ± 4.7 TgCH₄ yr⁻¹ from fossil fuel, 25.7 ± 10.9 TgCH₄ yr⁻¹ from wetlands, and 23.6 ± 5.8 TgCH₄ yr⁻¹ from agriculture and waste.

The posterior flux for total (anthropogenic and natural) land-atmosphere exchange of N₂O emissions was estimated as 2.3 ± 0.9 TgN₂O yr⁻¹ for North America (Figure 4), partitioned between the USA (1.6 ± 0.52 TgN₂O yr⁻¹), Canada (0.19 ± 0.11 TgN₂O yr⁻¹), Mexico (0.4 ± 0.2 TgN₂O yr⁻¹) and CA + CAR (0.1 ± 0.1 TgN₂O yr⁻¹).

3.5. Biospheric Carbon Exchange

The TRENDYv9 (S3) model ensemble estimated a regional land sink of $1,603 \pm 1445.1$ TgCO₂ yr⁻¹ for 2010–2019, an increase over 2000–2009 ($1,137.9 \pm 1,336.2$ TgCO₂ yr⁻¹), see Figure 5 for spatial distribution. Canada had the largest net carbon uptake (for 2010–2019) of 744.5 ± 479.9 TgCO₂, followed by the USA 695.4 ± 647.3 TgCO₂, Mexico (128.6 ± 221.7 TgCO₂) and CA + CAR (34.3 ± 96.2 TgCO₂). In contrast, the FluxCom (2010–2019) estimates were 4-times larger than the TRENDY models (Figure 7), 8,954.1 to 9,709.1 TgCO₂ yr⁻¹ for the RS and ERA5 approaches, respectively, and the SMOS based estimates were 28.4–272 TgCO₂ yr⁻¹. At the sub-regional scale, the differences with FluxCom being significantly higher and SMOS being lower than TRENDY was consistent. Biases in using FluxCom to estimate NBP have been addressed in

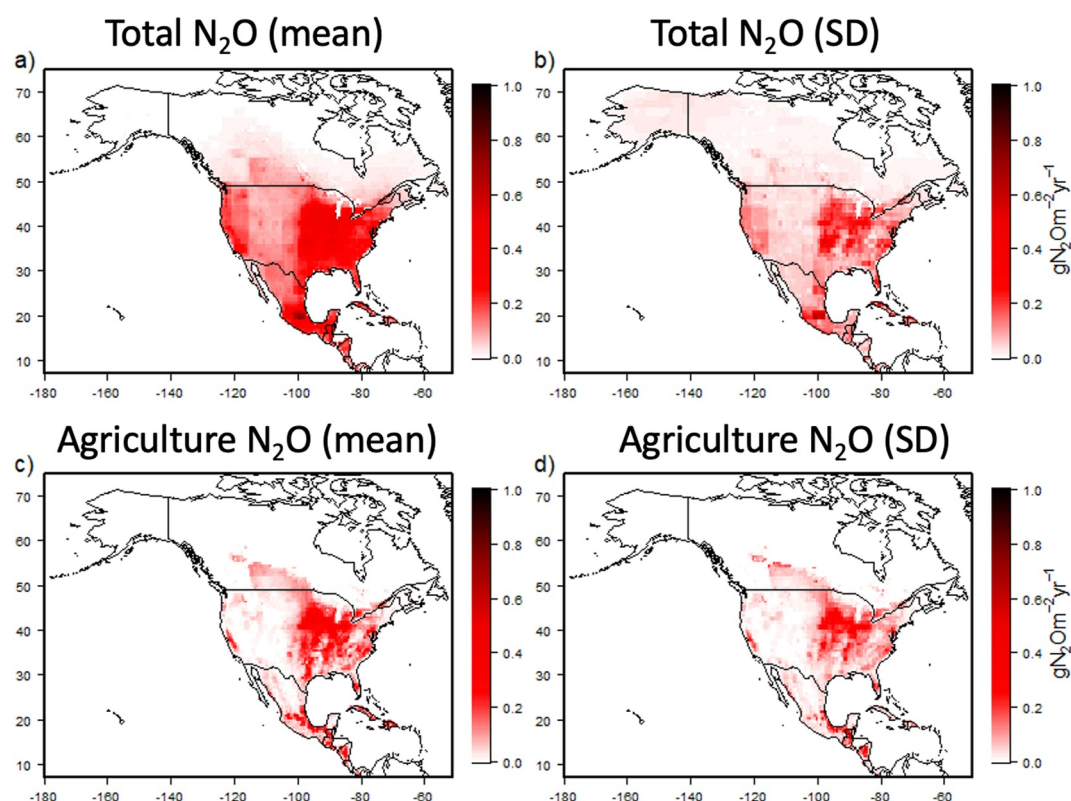


Figure 4. Total industrial and agricultural N_2O emissions and uncertainties (a and b) and agriculture emissions and uncertainties (c and d). Data gridded from the atmospheric inversion ensemble and posterior estimates (Tian et al., 2024).

previous literature (Zscheischler et al., 2017), and we evaluate the SMOS NBP estimate in the context of carbon stock change in following sections.

For North America, the NIR and BUR estimates of LULUCF estimated net removals of 1,037.3 (2000–2009) and 989.4 (2010–2019) $\text{TgCO}_2 \text{ yr}^{-1}$. The NIR/BUR net removals were higher than FAOSTAT, which estimated 397.9 (2000–2009) and 440.6 (2010–2019) $\text{TgCO}_2 \text{ yr}^{-1}$. Both the NIR/BUR and FAOSTAT estimates are more similar in sign and magnitude to the TRENDY S3 ensemble mean, and to some extent, the lower LULUCF estimate from the NIR/BUR can be explained by differences in the land-area used to estimate fluxes, for example, roughly two-thirds of the Canadian land base is considered unmanaged and excluded from the NIR (Ogle et al., 2018).

The WRIcf model, which combines remote-sensing data with IPCC Guidelines within a gain-loss framework, estimates a net regional sink of 1,551.1 $\text{TgCO}_2 \text{ yr}^{-1}$, with a sink for Canada of 726.3 $\text{TgCO}_2 \text{ yr}^{-1}$, the USA 662.0 $\text{TgCO}_2 \text{ yr}^{-1}$, Mexico 132.8 $\text{TgCO}_2 \text{ yr}^{-1}$, and CA + CAR 30.0 $\text{TgCO}_2 \text{ yr}^{-1}$. The WRIcf model produces similar magnitude to the TRENDY ensemble, in part because the managed land proxy for Canada is not used to mask out unmanaged lands.

3.6. Land Use and Land-Use Change Emissions

For the North American region (for 2010–2019), net LULUCF fluxes (Figure 6) were 193.7 $\text{TgCO}_2 \text{ yr}^{-1}$ from the NIRs, 772.5 \pm 967.9 TgCO_2 from the DGVM ensemble (i.e., S2–S3, Figure 8), and 20.7 \pm 279.4 TgCO_2 from the three bookkeeping models. The LULUCF emissions from CH_4 and N_2O were negligible and thus not reported here. The large differences between land-use change emission estimates have been explained by previous studies and attributed in part to (a) the NIR including most of ‘natural’ carbon fluxes (on managed lands) that is, the effects of climate and CO_2 fertilization on carbon uptake, (b) differences between the land-area considered managed by the NIR and other estimates, and (c) the DGVM emissions including the impact of loss of additional sink capacity. Compared to the LULUCF emissions, the deforestation emissions (i.e., excluding regrowth) are

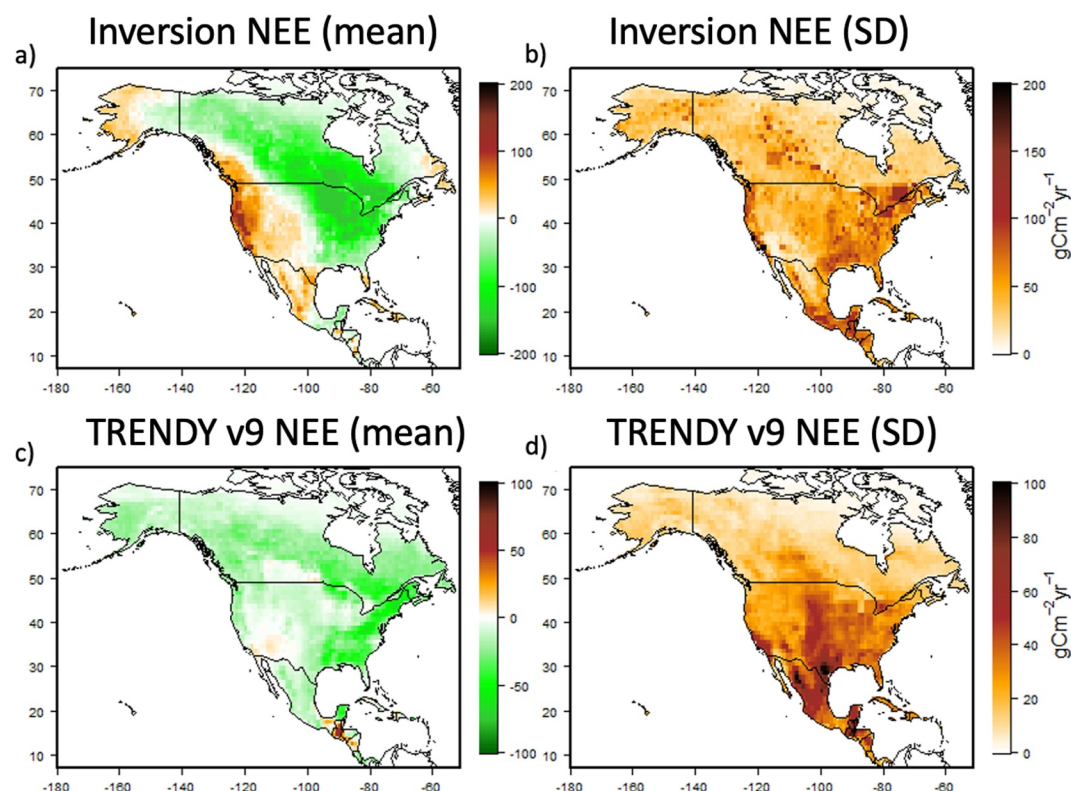


Figure 5. Annual average (2010–2019) net ecosystem exchange, NEE, for the Global Carbon Budget atmospheric inversion ensemble (a) and its uncertainties (b), and for the TRENDY land-surface model ensemble (c) and its uncertainties (d). Positive values indicate net carbon uptake from the atmosphere.

more similar between the NIR, bookkeeping models and FAOSTAT, ranging from $193.7 \text{ TgCO}_2 \text{ yr}^{-1}$ for the NIR and $71.8 \text{ TgCO}_2 \text{ yr}^{-1}$ for H&N, $568.1 \text{ TgCO}_2 \text{ yr}^{-1}$ for BLUE and $523.2 \text{ TgCO}_2 \text{ yr}^{-1}$ for OSCAR, and 189.7 TgCO_2 from FAOSTAT. The lower deforestation emissions for H&N is largely due to assumptions on how fire suppression led to increases in biomass on non-forested lands.

Accounting for the LASC reduced the DGVM LULUCF emissions from 772.5 ± 967.9 to $407 \pm 927.5 \text{ TgCO}_2 \text{ yr}^{-1}$. Between 2000–2009 and 2010–2019, no significant change in land-use change emissions estimated by the DGVMs (434.6 ± 696.9 vs. $407.0 \pm 927.5 \text{ TgCO}_2 \text{ yr}^{-1}$) or other approaches. We also use an alternative approach proposed by Grassi et al. (2023) and applied by Friedlingstein et al. (2023) in the Global Carbon Budget, to reconcile bookkeeping and NIR LULUCF emissions where the S2 NBP ensemble mean from TRENDY was subtracted from the bookkeeping ELUC emission estimates to account for natural fluxes not included in the bookkeeping models. Using this approach, we find more comparable estimates between the NIR and bookkeeping models for Mexico and the USA, but larger differences for Canada.

3.7. Vegetated Freshwater Wetland Emissions (CH_4)

For 2010–2019, North American vegetated wetland CH_4 emissions ranged from $19.5 \pm 2.9 \text{ TgCH}_4 \text{ yr}^{-1}$ to $21.5 \pm 10.1 \text{ TgCH}_4 \text{ yr}^{-1}$ based on the data-driven (UpCH₄) and process-model estimates (Figure 9). No significant increase between 2000–2009 and 2010–2019 was detectable given the large uncertainties. Highest emissions (2010–2019) were in Canada ($8.4 \pm 2.1 \text{ TgCH}_4 \text{ yr}^{-1}$ (UpCH₄) to $11.8 \pm 5.7 \text{ TgCH}_4 \text{ yr}^{-1}$ (wetland models)), followed by USA ($7.2 \pm 1.7 \text{ TgCH}_4 \text{ yr}^{-1}$ to $4.1 \pm 1.9 \text{ TgCH}_4 \text{ yr}^{-1}$), Mexico ($2.5 \pm 0.7 \text{ TgCH}_4 \text{ yr}^{-1}$ to $3.6 \pm 1.6 \text{ TgCH}_4 \text{ yr}^{-1}$), and CA + CAR ($1.5 \pm 0.6 \text{ TgCH}_4 \text{ yr}^{-1}$ to $2.0 \pm 1.0 \text{ TgCH}_4 \text{ yr}^{-1}$). Changes in the activity data used to estimate managed wetlands between the 2022 and 2023 NIR for the USA led to almost a doubling of wetland CH_4 emissions in “flooded lands” from 0.95 to 1.6 TgCH_4 and no change in emissions from “coastal wetlands” 0.15 TgCH_4 . The Canadian and USA NIR reports wetland CH_4 emissions, but only those emissions

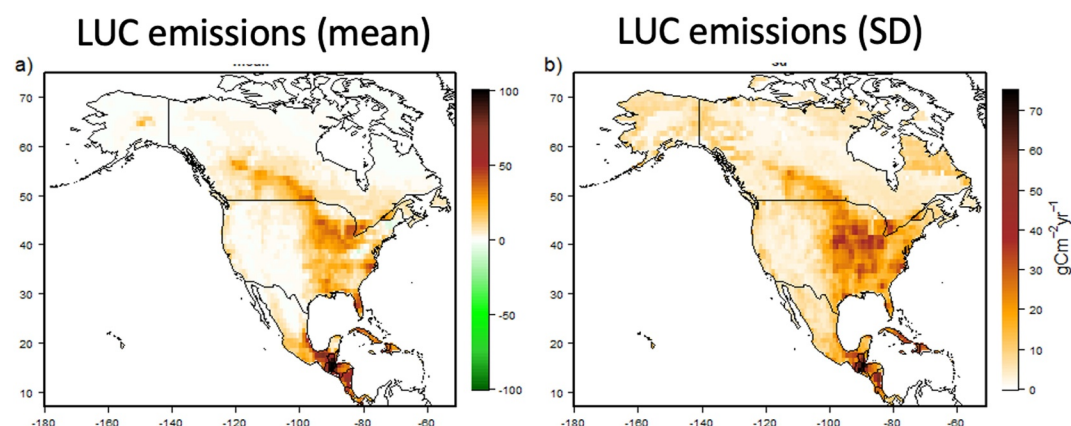


Figure 6. Land-use change emissions (2010–2019) and their uncertainties estimated from the TRENDYv9 model ensemble. The TRENDY S2 (no land use change) scenario is used as a reference and the S3 scenario has annually changed land cover and land use. The difference between S2 and S3 includes the emissions from land use change, but also the impacts from climate and CO₂ fertilization on biomass stocks between the two scenarios.

affected by anthropogenic activities and management and are not directly comparable with the wetland CH₄ model ensemble or UpCH₄.

3.8. Fluxes Across the Land-Ocean-Aquatic Continuum

Using a mass balance approach, we estimate the North American lateral carbon flux from land to inland waters (F_{li}) to range from 1,473 to 2,440 TgCO₂ yr⁻¹ (Figure 10). F_{li} is the sum of outgassing and evasive fluxes (F_{ia} = 418 to 1,385 TgCO₂ yr⁻¹), burial fluxes (F_{is} = 568 TgCO₂ yr⁻¹) within rivers and lakes, and export to estuaries (F_{ie} = 486 TgCO₂ yr⁻¹). In comparison, the SOCCR2 mass balance derived F_{li} was 1,854 TgCO₂ yr⁻¹.

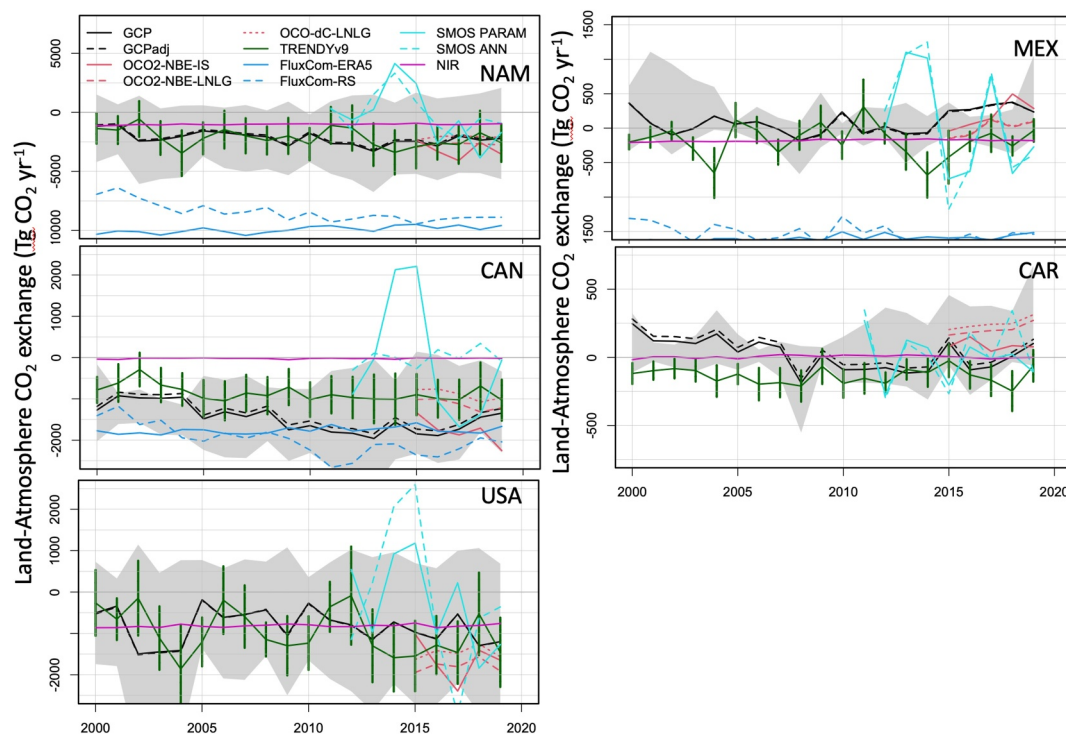


Figure 7. Land-atmosphere exchange of CO₂ for the North American region (NAM) and the four sub-regions. The figures contrast inventories, top-down, and bottom-up approaches, where negative indicate net CO₂ uptake and positive indicates net CO₂ release to the atmosphere. The difference in estimates is partly reconciled through adjustments for LOAC.

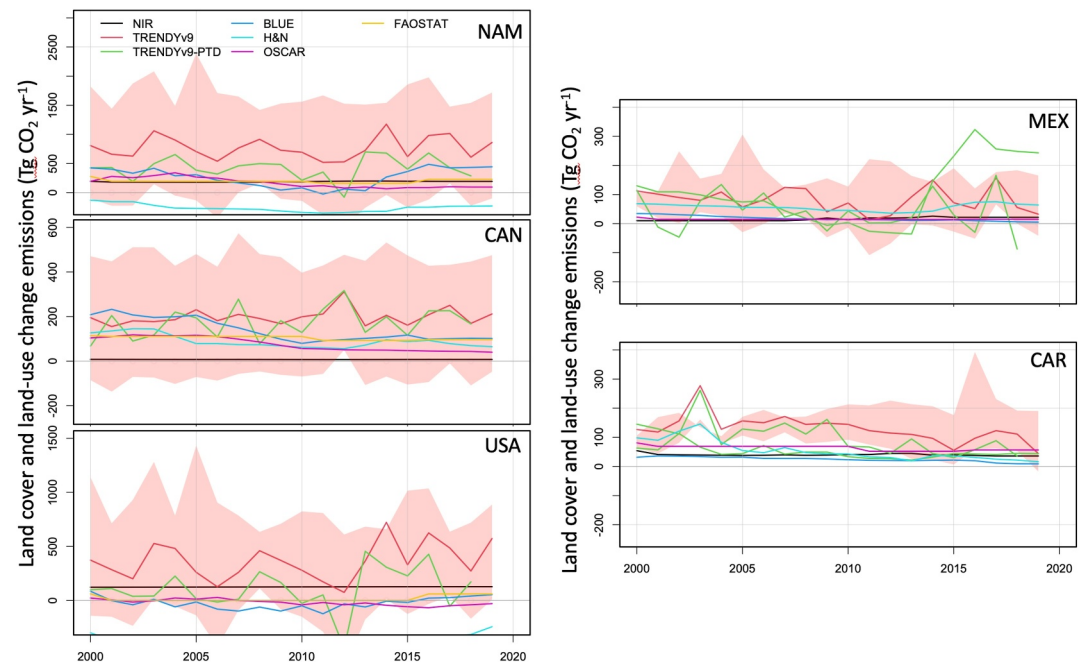


Figure 8. Land cover and land use change emissions for NAM and its four subregions. The figures contrast the differences between inventory estimates using gain-loss or stock change approaches (NIR, FAOSTAT), bookkeeping models (BLUE, OSCAR, H&N) and the process-based modeling methodologies (TRENDYv9). The red shading indicates uncertainty for the TRENDY v9 model ensemble, and the green line indicates the LASC correction applied to TRENDYv9.

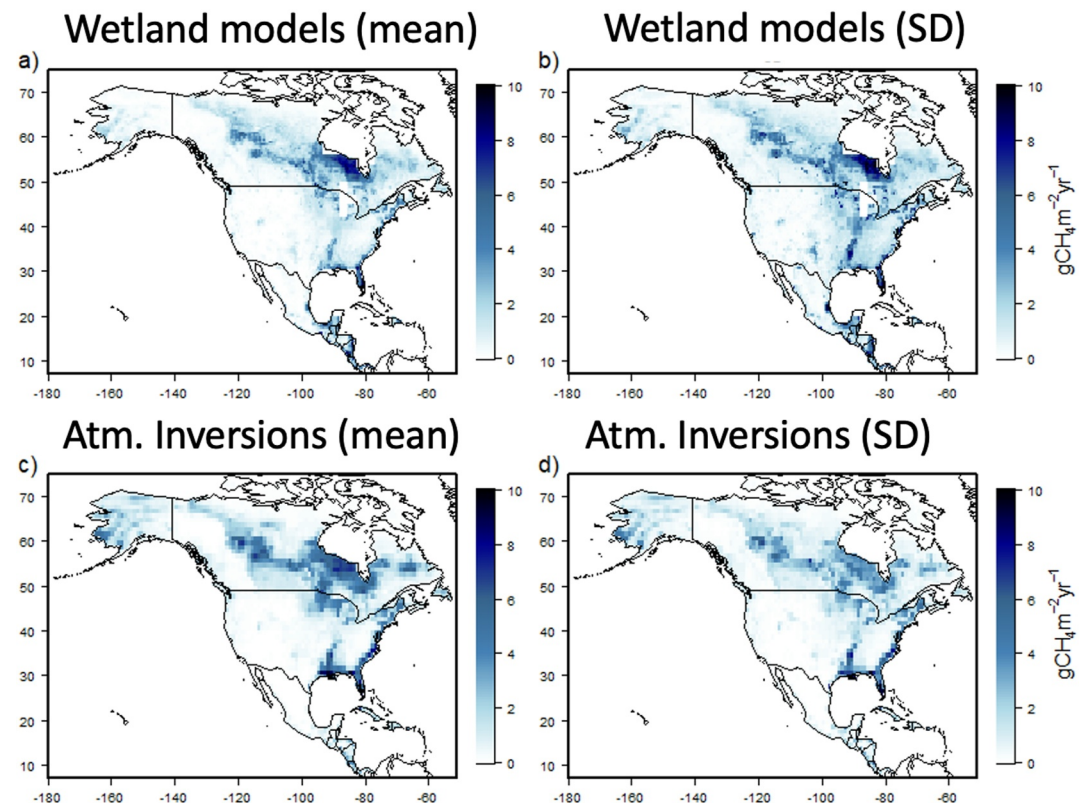


Figure 9. Wetland methane emissions from the Global Methane Budget (GMB) ensemble and their uncertainties (a and b) and from the GMB atmospheric inversions (c and d).

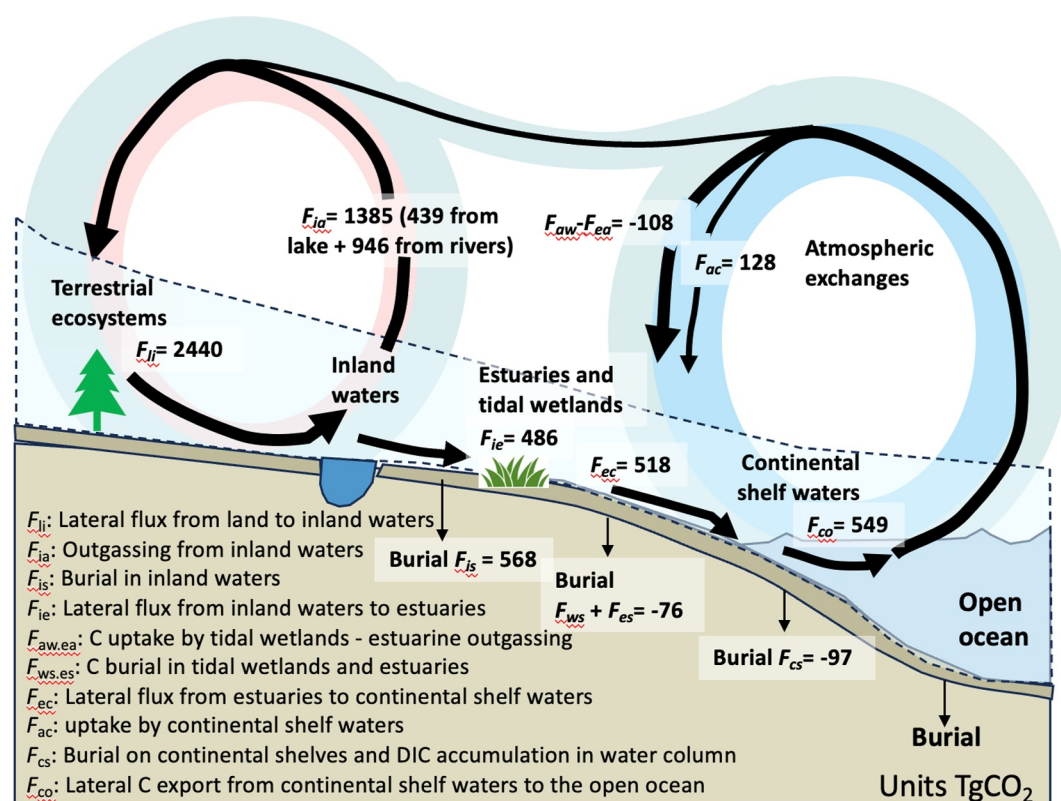


Figure 10. The land-to-ocean loops of the North American carbon cycle (2010–2019) derived from the independent estimates of LOAC fluxes. The long-range loop, lateral flux from land-to-ocean (F_{ie}) is $486 \text{ TgCO}_2 \text{ yr}^{-1}$, and defined by inputs, recycling and outputs of carbon from the land to aquatic systems. Figure adapted to use North America estimates from Regnier et al. (2022).

with 447 and $454 \text{ TgCO}_2 \text{ yr}^{-1}$ from lake and river evasion, $568 \text{ TgCO}_2 \text{ yr}^{-1}$ (burial) and $385 \text{ TgCO}_2 \text{ yr}^{-1}$ from export (Butman et al., 2018). The estimate for F_{ie} from Liu et al. (2024) is comparable to the GCB atmospheric inversion adjustment (see Methods *Top-down atmospheric inversions*), which estimated $370.2 \text{ TgCO}_2 \text{ yr}^{-1}$ for North America (149.1 , 135.3 , 33.1 , and $52.7 \text{ TgCO}_2 \text{ yr}^{-1}$ for Canada, USA, Mexico, CA + CAR) and OCO2-MIP ($437.4 \text{ TgCO}_2 \text{ yr}^{-1}$ for N America, 170.9 , 174.4 , 40.3 , 51.2). The differences resulting mainly from the Liu et al. (2024) estimate of F_{ie} including carbonate weathering ($\sim 93.7 \text{ TgCO}_2 \text{ yr}^{-1}$) and also that OCO2-MIP averaged two lateral flux estimates from Tian et al. (2010) and Deng et al. (2022). Uncertainties in total lake and river outgassing emissions range from minimum estimate of 418 to maximum estimate of $1,385 \text{ TgCO}_2 \text{ yr}^{-1}$ for North America, explaining a large part of the range in F_{li} , with the higher outgassing estimates more likely due to the inclusion of small streams and ponds. For North America, the lateral carbon export to estuaries to the continental shelf (F_{ec}) is thus $518 \text{ TgCO}_2 \text{ yr}^{-1}$; the sum of 486 (F_{ie}) — 76 ($F_{ws} + F_{es}$) — -108 ($F_{aw} + F_{ea}$).

The average North American evasive fluxes for lakes were 438.9 – $584 \text{ TgCO}_2 \text{ yr}^{-1}$, $29.7 \text{ TgCH}_4 \text{ yr}^{-1}$, and $0.02 \text{ TgN}_2\text{O yr}^{-1}$ and for rivers, 684 – $946.7 \text{ TgCO}_2 \text{ yr}^{-1}$, $4.1 \text{ TgCH}_4 \text{ yr}^{-1}$, and $6 \text{ Gg N}_2\text{O yr}^{-1}$. The highest total evasion rates were in Canada (710.0 TgCO_2 and 20.3 TgCH_4). Coastal systems net ecosystem exchange for mangroves, salt marshes and seagrasses removed -70.3 TgCO_2 from the atmosphere and emitted 0.2 TgCH_4 and close to zero N_2O emissions. The USA and Mexico had the highest coastal NEE, -36.8 and -32.7 TgCO_2 , respectively. Estuarine systems (fjords, lagoons, tidal deltas) also removed CO_2 from the atmosphere (-38 TgCO_2 , mainly from fjords), and emitted 0.11 TgCH_4 and $0.03 \text{ TgN}_2\text{O}$. Burial in lake, pond and reservoir sediments was estimated as -568 TgCO_2 , and burial in estuaries was estimated as $-76.4 \text{ TgCO}_2 \text{ yr}^{-1}$. Coastal margin and riverine inputs to the ocean were estimated as 447.3 and $370.3 \text{ TgCO}_2 \text{ yr}^{-1}$, and continental shelf burial $-96 \text{ TgCO}_2 \text{ yr}^{-1}$ and sea-air exchange as $128 \text{ TgCO}_2 \text{ yr}^{-1}$ with lateral carbon export from the continental shelf to open ocean (F_{co}) estimated at $549 \text{ TgCO}_2 \text{ yr}^{-1}$.

3.9. Harvest and Trade Fluxes for Crop and Wood Products

Total crop harvest from FAOSTAT was $1,757 \text{ TgCO}_2 \text{ yr}^{-1}$ for North America; $78.6 \text{ TgCO}_2 \text{ yr}^{-1}$ for Central America and Caribbean, $240.5 \text{ TgCO}_2 \text{ yr}^{-1}$ for Mexico, $1263.5 \text{ TgCO}_2 \text{ yr}^{-1}$ for the USA and $175.2 \text{ TgCO}_2 \text{ yr}^{-1}$ for Canada. Total wood harvest from FAOSTAT was $763.7 \text{ TgCO}_2 \text{ yr}^{-1}$ for North America; $107.9 \text{ TgCO}_2 \text{ yr}^{-1}$ for Central America and Caribbean, $21.5 \text{ TgCO}_2 \text{ yr}^{-1}$ for Mexico, $465.5 \text{ TgCO}_2 \text{ yr}^{-1}$ for the USA and $168.6 \text{ TgCO}_2 \text{ yr}^{-1}$ for Canada. Approximately 337.8 TgCO_2 of crops produced were exported and $129.8 \text{ TgCO}_2 \text{ yr}^{-1}$ of crops imported. Wood exports within the North American region were $161 \text{ TgCO}_2 \text{ yr}^{-1}$ and imports were $108.9 \text{ TgCO}_2 \text{ yr}^{-1}$. Total wood exports within and outside North America were $68.2 \text{ TgCO}_2 \text{ yr}^{-1}$ and for imports were $38.4 \text{ TgCO}_2 \text{ yr}^{-1}$, meaning that up to $90 \text{ TgCO}_2 \text{ yr}^{-1}$ were traded between the North American sub-regions. In contrast, OCO2-MIP assumed a net import of crops and wood products of $181.7 \pm -54.5 \text{ TgCO}_2 \text{ yr}^{-1}$ compared to our total net import estimate of $237.8 \text{ TgCO}_2 \text{ yr}^{-1}$.

We estimated crop consumption emissions by humans as $112.3 \text{ TgCO}_2 \text{ yr}^{-1}$ and livestock consumption emissions of $1,395.2 \text{ TgCO}_2 \text{ yr}^{-1}$ for a total consumption emissions of $1,507 \text{ TgCO}_2 \text{ yr}^{-1}$. The ratio of human to livestock consumption of crops is similar to Hayes et al. (2012) but smaller than the ratio estimated by Ciais et al. (2007). The remaining harvested crop carbon was emitted as CH_4 via enteric fermentation. Total landfill emissions of wood harvested products were estimated as $593 \text{ TgCO}_2 \text{ yr}^{-1}$, with a landfill pool size of 306.9 TgCO_2 and an end-use pool size of $10,075.9 \text{ TgCO}_2$. The NIRs do not provide gross wood harvest and product pool terms and instead provide a net CO_2 flux for harvested wood products. For the USA, the NIR estimated net uptake of carbon (-85.5 TgCO_2), a net loss for Canada (137.7 TgCO_2) and Mexico (52.2 TgCO_2).

The effect of crop harvest on atmospheric CO_2 concentrations is often considered net neutral because the biomass of crops is grown the same year (Hristov et al., 2018). For example, Hayes et al. (2012) estimated cropland NEE to be around $\sim 1,100 \text{ TgCO}_2 \text{ yr}^{-1}$ compared to the $\sim 1,700 \text{ TgCO}_2 \text{ yr}^{-1}$ crop harvest. Thus, we assume that the forward models, that is, DGVMs, include the crop regrowth in their NPP term and that the emissions of crop consumption to the atmosphere is included in the DGVM heterotrophic respiration term.

3.10. Other Fluxes and Stocks

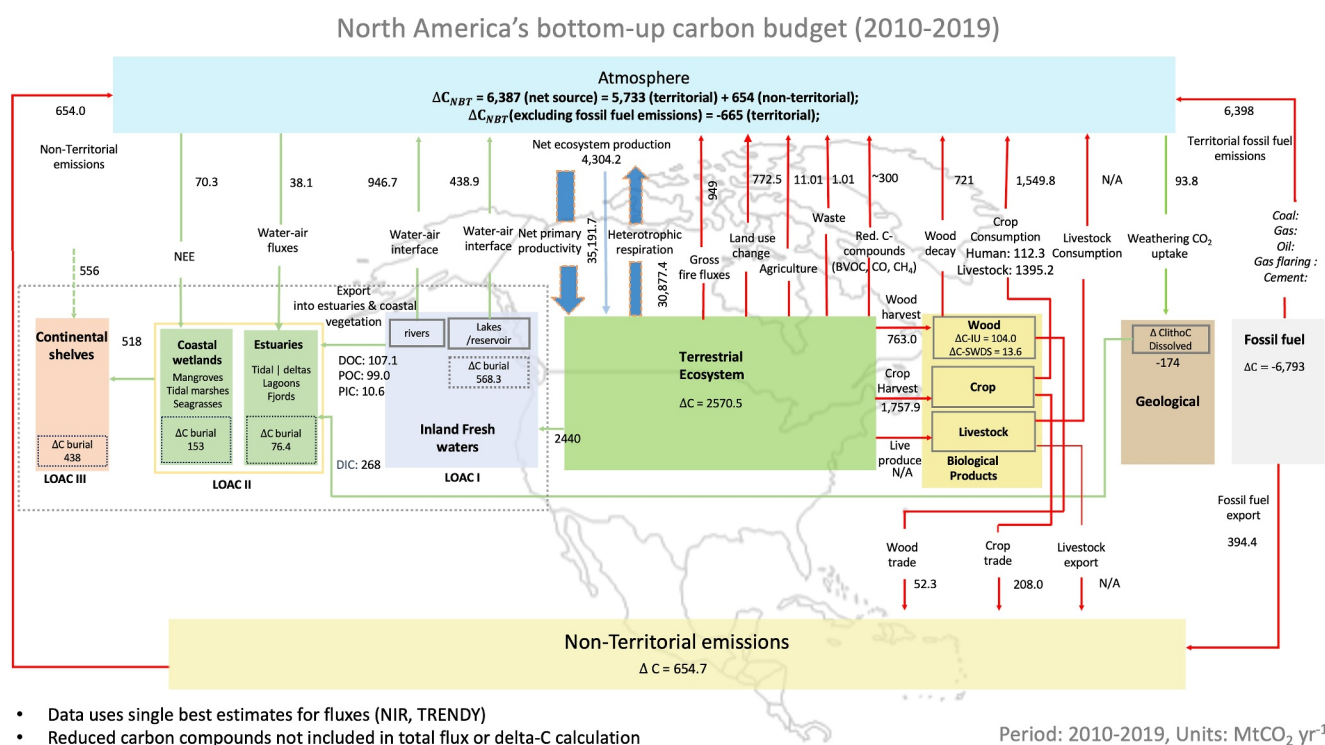
North American standing carbon stocks ranged from 26.2 PgC ($1 \text{ Pg} = 1,000 \text{ Tg}$) (ESA CCI), 33.9 PgC (FAOSTAT), and $74.5 \pm 35.1 \text{ PgC}$ (TRENDYv9). By country, the remote-sensing based estimates ranged from 10.5 to 21.0 PgC for Canada, 16.5 to 21.4 PgC for the USA, 2.3 to 4.2 PgC for Mexico and 2.9 PgC for CA + CAR. Soil carbon stocks ranged from $289 \pm 190.7 \text{ PgC}$ (TRENDY) to 511 PgC (SoilGrids 0–200 cm). With highest soil carbon stocks, for SoilGrids, in Canada (269.1 PgC), then the USA (191 PgC), Mexico (31.9 PgC), and CA + CAR (18.3 PgC).

For carbon fluxes, BVOC emissions from CAMS were estimated as $250 \text{ TgCO}_2 \text{ yr}^{-1}$, with $34.8 \text{ TgCO}_2 \text{ yr}^{-1}$ from Canada, $120.9 \text{ TgCO}_2 \text{ yr}^{-1}$ from the USA, $61.0 \text{ TgCO}_2 \text{ yr}^{-1}$ from Mexico, and $33.8 \text{ TgCO}_2 \text{ yr}^{-1}$ from CA + CAR. Regional CO_2 emissions from fire were 447.9 – $502.9 \text{ TgCO}_2 \text{ yr}^{-1}$ (GFED and QFED). Regional GPP was $70,855 \pm 13,678 \text{ TgCO}_2 \text{ yr}^{-1}$ (TRENDYv9) and $54,500$ – $55,571 \text{ TgCO}_2 \text{ yr}^{-1}$ (FluxCom), $67,894 \text{ TgCO}_2 \text{ yr}^{-1}$ (FluxSat), and $66,230 \text{ TgCO}_2 \text{ yr}^{-1}$ (GOSIF).

3.11. Net GHG Emissions

The net BU (anthropogenic and natural) 2010–2019 emissions for North America were $6,387 \text{ TgCO}_2 \text{ yr}^{-1}$, and of this amount, $5,733 \text{ TgCO}_2 \text{ yr}^{-1}$ was from territorial emissions and an additional $654 \text{ TgCO}_2 \text{ yr}^{-1}$ from non-territorial emissions (Figure 11). This is equal to roughly a 0.9 ppm yr^{-1} increase in atmospheric CO_2 concentration ($1 \text{ ppm} = 2,124 \text{ TgC}$ ($7,788 \text{ TgCO}_2$); Friedlingstein et al. (2023)). Net territorial emissions for Canada were $507 \text{ TgCO}_2 \text{ yr}^{-1}$ (Figure S1 in Supporting Information S1), $4,522 \text{ TgCO}_2 \text{ yr}^{-1}$ for the USA (Figure S2 in Supporting Information S1), $372 \text{ TgCO}_2 \text{ yr}^{-1}$ for Mexico (Figure S3 in Supporting Information S1) and $331 \text{ TgCO}_2 \text{ yr}^{-1}$ for CA + CAR (Figure S4 in Supporting Information S1). Net CO_2 emissions declined compared to the previous decade, where the 2000–2009 net territorial CO_2 emissions were $6,757 \text{ TgCO}_2 \text{ yr}^{-1}$. The reduction was mainly due to lower territorial emissions in the USA ($5,299$ – $4,522 \text{ TgCO}_2 \text{ yr}^{-1}$) coming from a $520 \text{ TgCO}_2 \text{ yr}^{-1}$ reduction in fossil emissions.

Total net TD territorial emission estimates for North America were $4,733 \pm 2,942 \text{ TgCO}_2 \text{ yr}^{-1}$ (2009–2010) and $3,806 \pm 2,949 \text{ TgCO}_2 \text{ yr}^{-1}$ (2010–2019) using the GCB ensemble and GridFED, and similar to the OCO2-MIP



- Data uses single best estimates for fluxes (NIR, TRENDY)
- Reduced carbon compounds not included in total flux or delta-C calculation

Figure 11. Integrated bottom-up CO₂ budget for North America (2010–2019). Red arrows are anthropogenic flows of carbon and green arrows are natural flows. Direction of arrow indicates whether carbon is being removed or entering the atmosphere. Dashed arrows indicate the number is not used to estimate the stock change. The numbers used in the budget are available through the “wiring diagram-CO₂” tab of the data file. Figures S1–S4 in Supporting Information S1 provide the regional breakdowns for Canada, United States, Mexico and Central America. Figure adapted from Villalobos et al. (2023).

LNLG satellite-based estimate of $3,360 \pm 1,981$ TgCO₂ yr⁻¹ (2015–2019). Based on GCB and GridFED, territorial emissions were $-1,149 \pm 1,071$ TgCO₂ yr⁻¹ for Canada, $4,385 \pm 1,512$ TgCO₂ yr⁻¹ for the USA, 308 ± 357 TgCO₂ yr⁻¹ for Mexico, and 99 ± 168 TgCO₂ yr⁻¹ for CA + CAR. Part of the difference between BU and TD can be explained by the lake and river evasion estimates in the BU approach and highlights the importance of accounting for lateral LOAC fluxes, which are not included in Equation 1 and also the larger NEP estimated by the inversions for Canada.

The bottom-up dCH₄atm for 2010–2019 was 99.5 TgCH₄ yr⁻¹ compared to top-down emissions of 65.8 TgCH₄ yr⁻¹ (Figure 12, where thermogenic emissions represent emissions from oil, gas, coal activities, and pyrogenic emissions from wildfire and biomass burning). For each of the four subregions, BU emissions were 37.2 versus TD 18.0 TgCH₄ yr⁻¹ for Canada (Figure S5 in Supporting Information S1), 48.7 BU versus TD 39.8 TgCH₄ yr⁻¹ for the USA (Figure S6 in Supporting Information S1), 9.8 BU versus TD 5.1 TgCH₄ yr⁻¹ for Mexico (Figure S7 in Supporting Information S1) and 5.0 BU versus TD 2.8 TgCH₄ yr⁻¹ for CA + CAR (Figure S8 in Supporting Information S1). Compared to 2000–2009, BU regional and sub-regional CH₄ emissions were similar (total: 102 ± 7 TgCH₄ yr⁻¹) to 2010–2019 emissions.

The bottom-up dN₂Oatm emissions (2010–2019) were $1,924$ GgN₂O yr⁻¹ compared to TD emissions of $2,328$ GgN₂O yr⁻¹ for North America (Figure 13). Canada's emissions were 189 (BU) versus 192 (TD) GgN₂O yr⁻¹ (Figure S9 in Supporting Information S1), and $1,521$ versus $1,611$ GgN₂O yr⁻¹ for the USA (Figure S10 in Supporting Information S1), 321.1 versus 420.9 GgN₂O yr⁻¹ for Mexico (Figure S11 in Supporting Information S1), and 65 versus 105 GgN₂O yr⁻¹ for CA + CAR (Figure S12 in Supporting Information S1). Between 2000 and 2019, N₂O emissions increased by 80 GgN₂O yr⁻¹.

3.12. GWP-100 Years Horizon Budgets (CO₂-eq)

For North America, the net TD territorial budget over 100 years horizon was $7,169 \pm 1,832$ TgCO₂-eq yr⁻¹ for 2000–2009 and $6,132 \pm 1,846$ TgCO₂-eq yr⁻¹ for 2010–2019. The BU territorial budget over 100 years horizon

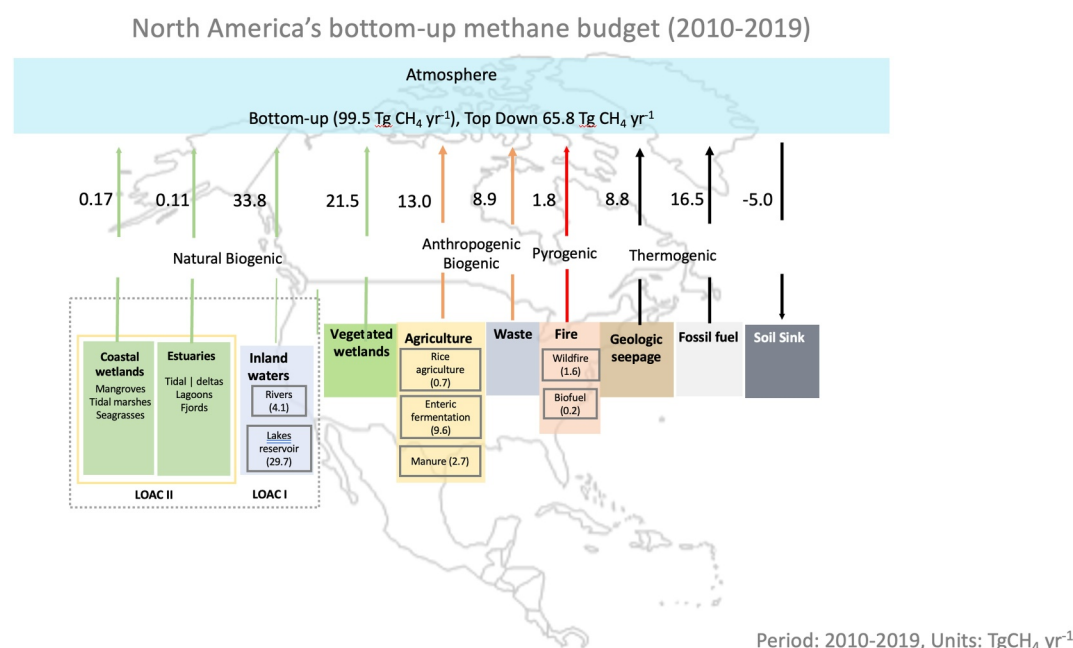


Figure 12. Integrated bottom-up CH₄ budget for North America (2010–2019). See Figures S5–S8 in Supporting Information S1 for regional breakdown.

was $9,989 \pm 898$ TgCO₂-eq for 2000–2009 and $9,060 \pm 898$ TgCO₂-eq for 2010–2019. By sub-region, for 2010–2019, TD and BU emissions were -636 ± 913 and $1,608 \pm 504$ TgCO₂-eq yr⁻¹ for Canada, $5,724 \pm 1,552$ and $6,195 \pm 698$ TgCO₂-eq yr⁻¹ for the USA, 848 ± 363 and 734 ± 140 TgCO₂-eq yr⁻¹ for Mexico, and 196 ± 177 and 521 ± 114 TgCO₂-eq yr⁻¹ for Central America and the Caribbean (Table 1). The difference between the TD and BU estimates, $\sim 3,000$ TgCO₂-eq yr⁻¹, is largely explained by estimates for Canada, where the BU estimate was $\sim 2,000$ TgCO₂-eq yr⁻¹ larger than TD. Part of the difference is due to the larger Canadian CO₂ sink estimate provided by the TD approach. In addition, higher BU CH₄ emissions for Canada (likely from double counting the wetland and inland-water sources) and for the USA also explains part of the difference between 2010 and 2019 TD CH₄ emissions ($1,613 \pm 266$ TgCO₂-eq yr⁻¹) compared to BU emissions ($2,852 \pm 191$ TgCO₂-eq yr⁻¹).

Accounting for lateral fluxes from the LOAC and from trade helps to reconcile the BU and TD GHG budgets. To illustrate this, we use the estimates of Liu et al. (2024) for the lateral flux of total carbon from inland waters to estuaries (F_{ie}) of 486 TgCO₂ yr⁻¹, the WPsCS model for net wood trade exports (30 TgCO₂ yr⁻¹) and FAOSTAT for net crop trade exports (208 TgCO₂ yr⁻¹). These estimates are similar to those used in OCO2-MIP, which estimated 437 ± 264 TgCO₂ yr⁻¹ for F_{ie} and 181 ± 54 TgCO₂ yr⁻¹ for trade flows. Combined, the lateral fluxes account for 724 TgCO₂ yr⁻¹, which accounts for one third of the difference between the TD and BU approaches. Further reconciling of the TD and BU approaches can be carried out using the LASC correction applied to the land use change estimate in the DGVM models, which accounts for a ~ 400 TgCO₂ yr⁻¹ reduction in emissions by 2019.

The BU and TD budgets are similar to the NGHGI submitted to the UNFCCC, which estimate total net emissions of $7,270$ TgCO₂-eq yr⁻¹ for 2010–2019, a 6% decline from $7,756$ TgCO₂-eq yr⁻¹ for 2000–2009. The NGHGI follow the IPCC Guidelines (2006, 2019) and report emissions and removals only for managed lands. Thus, compared to TD approaches, the NGHGI net emissions are larger because they exclude large areas of removals in unmanaged forests in Canada. Compared with BU methods, the net-emissions reported by the NGHGI is lower, mainly because of the inclusion of emissions from inland water and unmanaged wetland ecosystems.

4. Discussion

Our assessment of the North America GHG budget provides a comprehensive update of GHG emissions and removals for all sectors including managed and unmanaged lands. The work provides an extension of all three main GHGs in time to the year 2019 following on other regional GHG assessments made by the North American

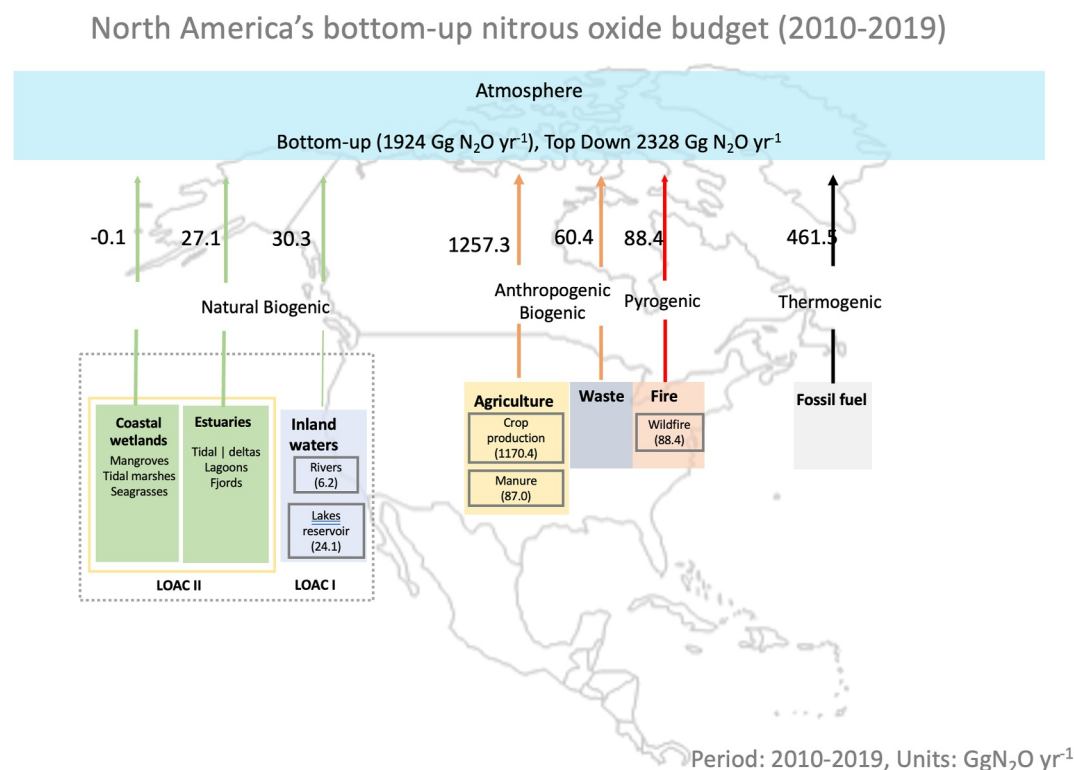


Figure 13. Integrated bottom-up N₂O budget for North America (2010–2019). See Figures S9–S12 in Supporting Information S1 for regional breakdown.

Carbon Program (NACP) (2000–2006; (Hayes et al., 2012)), RECCAP1 (1990–2009; (King et al., 2015)) and SOCCR2 (2004–2013; (Birdsey et al., 2018)), U.S. Geological Survey, USGS (2005–2014; (Merrill et al., 2018)) and OCO2MIP (2015–2019; (Byrne et al., 2023)). The approach incorporates a diverse set of data as well as methods for integrating lateral fluxes from the LOAC and trade, harmonizing LULUCF emissions, and addressing double counting. This is the first multi-GHG gas syntheses study for North America, with previous multi-gas studies carried out for the European region (Petrescu et al., 2021, 2023; Schulze et al., 2009, 2010) and

Table 1

Regional Breakdown of Total Anthropogenic and Non-Anthropogenic Net Greenhouse-Gas Emissions for Each Gas in Units of TgCO₂-eq (GWP-100)

| Method | | Canada | | United States | | Mexico | | CA and Caribbean | | North America | |
|-----------|---------------------|--------|--------|---------------|-------|--------|------|------------------|------|---------------|-------|
| | | 2000 | 2009 | 2010 | 2019 | 2000 | 2009 | 2010 | 2019 | 2000 | 2019 |
| NGHGI | CO ₂ | 547 | 553 | 5,147 | 4,596 | 259 | 341 | NA | 148 | 6,103 | 5,640 |
| | CH ₄ | 132 | 124 | 794 | 757 | 47 | 68 | 21 | 21 | 995 | 970 |
| | N ₂ O | 29 | 27 | 423 | 421 | 38 | 42 | 167 | 167 | 658 | 658 |
| | CO ₂ -eq | 707 | 705 | 6,366 | 5,775 | 345 | 452 | 336 | 336 | 7,756 | 7,270 |
| Top-Down | CO ₂ | −671 | −1,133 | 4,876 | 4,295 | 463 | 616 | 210 | 105 | 4,878 | 3,833 |
| | CH ₄ | 470 | 444 | 1,037 | 989 | 119 | 116 | 71 | 53 | 1,699 | 1,613 |
| | N ₂ O | 24 | 29 | 138 | 141 | 41 | 52 | 15 | 15 | 591 | 636 |
| | CO ₂ -eq | −148 | −636 | 6,323 | 5,724 | 686 | 848 | 307 | 196 | 7,169 | 6,132 |
| Bottom-Up | CO ₂ | 1,017 | 866 | 5,499 | 4,722 | 420 | 380 | 377 | 320 | 7,314 | 6,289 |
| | CH ₄ | 1,019 | 1,048 | 1,330 | 1,356 | 271 | 280 | 157 | 167 | 2,779 | 2,852 |
| | N ₂ O | 41 | 53 | 320 | 316 | 69 | 82 | 23 | 23 | 453 | 475 |
| | CO ₂ -eq | 2,078 | 1,967 | 7,150 | 6,395 | 759 | 743 | 557 | 510 | 10,546 | 9,616 |

Note. Numbers in italics are the sum of the three trace gases.

now as part of RECCAP2 for Africa (Ernst et al., 2024), Central Asia (Wang et al., 2024) and Australasia (Villalobos et al., 2023).

Few studies have evaluated the full GWP of emissions of North America for the three gases and across all anthropogenic and natural sectors. Our study shows that the inclusion of multiple data sets used to provide activity data, emissions factors, and direct flux estimates, can be used to infer more detailed information on GHG emissions and removals than provided in the NGHGI, and that the results are comparable after accounting for lateral flows, definitions, and double counting. Lateral fluxes were first identified by Pacala et al. (2001) as key for TD and BU reconciliation, and RECCAP1 and RECCAP2 have helped quantify these fluxes through development of new data sets along the continuum. For North America, the inland water outgassing of CO₂ and CH₄ from inland waters remains fairly uncertain, as well as carbon burial rates within rivers and streams, leading to fairly high estimates of F_{li} (lateral flux from land to inland waters) of 1,440–2,440 TgCO₂, which is roughly half of the North American NEP (4,304 TgCO₂ yr^{−1}). The uncertainties are partly related to mapping of small streams and ponds, limited empirical data along stream reaches, seasonally and year-to-year to use in scaling, which leads to double counting when combined with bottom-up estimates from other sectors, that is, vegetated wetlands.

Reconciling land-use change fluxes between bookkeeping, process-models, and inventories has been addressed in detail previously by Grassi et al. (2021, 2023) and Obermeier et al. (2021) and implemented now as part of the annual global carbon budget (Friedlingstein et al., 2022, 2023). The adjustment to the bookkeeping models using the S2 scenario to better match the definition of the NIR has been shown to work at national levels (Schwingshackl et al., 2022), making this approach promising for attribution studies. Additional work is needed to provide spatially aggregated information on LULUCF and AFOLU emissions and removals, where a mix of spatial scales, terminologies, and definitions for land classes (i.e., IPCC vs. plant functional types), and reporting areas still need to be addressed. In particular, grassland and settlement categories have high uncertainties in distribution, allometries, and soil carbon data (McGlynn et al., 2022). The use of remote sensing data sets and integration with the IPCC methodology would help provide this spatial disaggregation and consistency between inventory approaches, and the WRIcf model may help further advance these integrations.

Ongoing activities and opportunities to reconcile top-down and bottom-up approaches will help reduce the biases and uncertainties identified in this study. The NGHGI's presented here use a combination of Tier 1, 2, and 3 methodologies to estimate emissions and removals following IPCC Guidelines. These Tiers are designed to support country participation in developing NGHGI while maintaining Transparency, Accuracy, Consistency, Completeness, and Comparability (TACCC). The integration of new remote sensing products will help countries move toward Tier 3 methods (lower uncertainty using regional to sub-regional data) by constraining emissions from oil and gas activities, landfills, wildfire, and estimates of forest carbon stocks (e.g., Hunka et al., 2024), as well as provide improved and more consistent information for activity data used to estimate transitions in land use and land cover, the distribution of managed wetlands, and different agricultural practices.

While CO₂ fossil emissions decreased for the North America, due in large part to a decrease of 329–560 TgCO₂ yr^{−1} in the USA, fossil-related emissions from non-CO₂ GHGs increased. From 2000 to 2009 to 2010–2019, the ratio of non-CO₂-eq to total CO₂-eq emissions increased by about 1%. Emissions of non-CO₂ fossil gases remain uncertain, with the USA NIR showing a decrease from 12.7 TgCO₂-eq yr^{−1} to 11.9 TgCO₂-eq yr^{−1}, GAINS showing an increase over 10.5 to 10.3 TgCH₄ yr^{−1}, and IEA having a large estimate of 17 TgCH₄ yr^{−1} for the USA. This is equivalent to around 100–150 TgCO₂-eq yr^{−1} uncertainty for GWP-20. It is expected that oil and gas point-source emission uncertainties will decrease as atmospheric inventories incorporate an increasing volume of satellite information from plume mappers (Lu et al., 2023).

Natural disturbances driven fluxes from fire, hydrologic events, insects, windthrow, and disease are challenging to compare across data sets, partly because the country-level inventories each handles these differently, and partly because there are few consistent data sets available, especially for insects, windthrow and disease. While fire emission modeling is fairly advanced at global scales, with GFED and QFED having been developed in the early 2000s (Van der Werf et al., 2003) recent work has pointed to the importance of spatial resolution being a key driver of fire emission uncertainty (Ramo et al., 2021). To a certain extent, disturbance emissions are implicitly accounted for in the forest inventory, for example, in the case of the USA, the stock changes estimated from the forest-inventory analysis plots include losses of carbon from disturbance. For Canada, the fire-related emissions are reported separately, but the area included in estimating fire emissions can change year-to-year based on guidelines for when fire is natural or not.

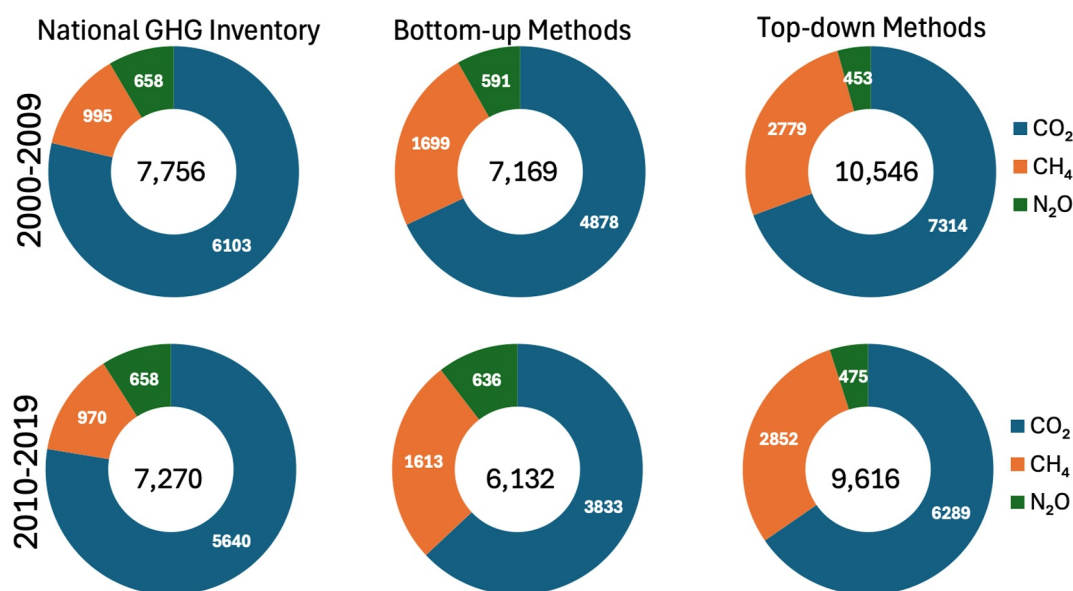


Figure 14. Distribution of anthropogenic, managed-lands and natural net greenhouse gas emissions (TgCO₂-eq yr⁻¹) for the entire North American region for 2000–2009 (upper panel) and 2010–2019 (lower panel). The columns (from left to right) contrast the national greenhouse gas inventory methods with the bottom-up and top-down methods.

The tracking of GHG emissions and removals is necessary to help understand the sources of anthropogenic GHGs, the success and effectiveness of mitigation, and to document whether climate or other feedbacks are weakening the land and ocean carbon sinks or changing the chemical sinks. For example, global anthropogenic emissions of CO₂ reached a record high in 2023 (Friedlingstein et al., 2023) and the atmospheric growth rate of CH₄ doubled in 2020 to a sustained growth rate of more than 10 ppb yr⁻¹ (Peng et al., 2022). Existing monitoring and reporting frameworks currently provide different perspectives on GHG emissions and removals depending on the methodology and policy frameworks they follow. The RECCAP2 activity is designed to help understand differences in reporting structures and to provide a framework for reconciling their differences.

5. Conclusions

This paper is one of the 10 regional land assessments contributing to the RECCAP2 assessment providing decadal multi-GHG gas budgets for two decades: 2000–2009 and 2010–2019. Multiple independent and quasi-independent data sets and methodologies are used to compare emissions and removals across anthropogenic and natural sectors. We find that the North America TD and BU approaches are net sources of GHGs and are in agreement with the NGHGI, with net emissions decreasing by 6%–14% between 2000–2009 and 2010–2019 (Figure 14) due mainly to reduction in fossil CO₂ emissions. Reconciling the differences between TD, BU and NGHGI approaches requires accounting for lateral flows from the LOAC and trade, reducing uncertainty in land-use change emissions, addressing double counting in inland-water CH₄ emissions, and reducing uncertainty in inland-water CO₂ evasion. The North America budget relied heavily on globally parameterized data sets, and we suggest advancing the development of regional inversion and land-surface models to better capture vegetation dynamics, disturbance drivers, regional soil properties (e.g., permafrost), wind transport, and take advantage of regional measurement networks.

List of Key Acronyms

| | |
|-------|--|
| AFOLU | Agriculture, Forestry and Other Land Use |
| BU | Bottom up |
| BUR | Biennial Update Report |

| | |
|---------------------|---|
| CH ₄ | Methane |
| CO ₂ | Carbon dioxide |
| CO ₂ -eq | Carbon dioxide equivalent |
| CRF | Common Reporting Format |
| GCB | Global Carbon Budget |
| GCP | Global Carbon Project |
| GHG | Greenhouse Gas |
| Gg | Gigagram |
| GMB | Global Methane Budget |
| GWP | Global Warming Potential |
| IPCC | Intergovernmental Panel on Climate Change |
| IPPU | Industrial Processes and Product Use |
| LASC | Loss of Additional Sink Capacity |
| LOAC | Land ocean aquatic continuum |
| LULUCF | Land use, land cover, and forestry |
| MMRV | Measurement, Monitoring, Reporting and Verification |
| MMT | Million metric tonnes |
| NACP | North American Carbon Program |
| NASA | National Aeronautics and Space Administration |
| NBP | Net biome production |
| NEE | Net ecosystem exchange |
| NEP | Net ecosystem production |
| NGHGI | National Greenhouse Gas Inventory |
| N ₂ O | Nitrous oxide |
| NIR | National Inventory Report |
| NMIP | Nitrogen Model Intercomparison Project |
| OCO | Orbiting Carbon Observatory |
| RECCAP2 | REgional Carbon Cycle Assessment and Processes study |
| SOCCR-2 | State of the Carbon Cycle Report |
| TD | Top down |
| Tg | Teragram |
| TRENDY | Trends in the Carbon Cycle |
| UNFCCC | United Nations Framework Convention on Climate Change |
| USA | United States of America |
| USDA | United States Department of Agriculture |

Data Availability Statement

Data are available from Poulter (2025) in an Excel file describing emissions and removals for each sector, data source and type of gas, and for each year (from 2000 to 2019), and by sub-region at <https://doi.org/10.5281/zenodo.14940052>.

Acknowledgments

During the development of the North America RECCAP2 assessment we appreciate inputs from Leonardo Calle, Giacomo Grassi, Charlie Koven, Gavin McNicol, Ahtziri Arreola Martinez, Julia Pongratz and Yoichi Shiga. Benjamin Poulter acknowledges support from NASA's Terrestrial Ecology Program and NASA's Carbon Monitoring System (CMS). Guillermo Murray thanks Universidad Nacional Autónoma de México for funding through project DGAPA PAPIIT IA200722. Robbie Andrew acknowledges support from the European Union's Horizon Europe research and innovation programme under Grant Agreement Numbers 10108139 (EYE-CLIMA) and 958927 (CoCO2). Dan Hayes and Xinyuan Wei acknowledge NASA CMS (80NSSC21K0966). Work of Abhishek Chatterjee was carried out at the Jet Propulsion Laboratory, California Institute of Technology, under a contract with the National Aeronautics and Space Administration (80NM0018D0004) and through Grant 80NSSC20K0006. Maodian Liu acknowledges NSFC (41977311) and Fundamental Research Funds for the Central Universities (7100604309). NRF, JCSN and AM acknowledge partial support by the ESA contract No. AO/1-10908/21/NL/IA (10 Years of SMOS—Passive Microwave Vegetation Opacity Study (PM-VO-S)) and from CNES (Centre National d'Etudes Spatiales) TOSCA program project SMOS-TE. Any use of trade, firm, or product names is for descriptive purposes only and does not imply endorsement by the U.S. Government.

References

- Alvarez, R. A., Zavala-Araiza, D., Lyon, D. R., Allen, D. T., Barkley, Z. R., Brandt, A. R., et al. (2018). Assessment of methane emissions from the U.S. oil and gas supply chain. *Science*, 361(6398), 186–188. <https://doi.org/10.1126/science.aar7204>
- Andrew, R. M. (2020). A comparison of estimates of global carbon dioxide emissions from fossil carbon sources. *Earth System Science Data*, 12(2), 1437–1465. <https://doi.org/10.5194/essd-12-1437-2020>
- Auch, R. F., Wellington, D. F., Taylor, J. L., Stehman, S. V., Tollerud, H. J., Brown, J. F., et al. (2022). Conterminous United States land-cover change (1985–2016): New insights from annual time series. *Land*, 11(2), 298. <https://doi.org/10.3390/land11020298>
- Battin, T. J., Lauerwald, R., Bernhardt, E. S., Bertuzzo, E., Gener, L. G., Hall, R. O., et al. (2023). River ecosystem metabolism and carbon biogeochemistry in a changing world. *Nature*, 613(7944), 449–459. <https://doi.org/10.1038/s41586-022-05500-8>
- Birdsey, R., Mayes, M. A., Romero-Lankao, P., Najjar, R., Reed, S. C., Cavallaro, N., et al. (2018). Executive summary. In *Second state of the carbon cycle report*. U.S. Global Change Research Program. <https://doi.org/10.7930/Soccr2.2018.ES>
- Bunting, P., Rosenqvist, A., Lucas, R. M., Rebelo, L.-M., Hilarides, L., Thomas, N., et al. (2018). The global mangrove watch—A new 2010 global baseline of mangrove extent. *Remote Sensing*, 10(10), 1669. <https://doi.org/10.3390/rs10101669>
- Butman, D., Striegl, R., Stackpole, S., del Giorgio, P., Prairie, Y., Pilcher, D., et al. (2018). Chapter 14: Inland waters. In N. Cavallaro, G. Shrestha, R. Birdsey, M. A. Mayes, R. G. Najjar, S. C. Reed, et al. (Eds.), *Second state of the carbon cycle report (SOCCR2): A sustained assessment report* (pp. 568–595). U.S. Global Change Research Program. <https://doi.org/10.7930/Soccr2.2018.Ch14>
- Byrne, B., Baker, D. F., Basu, S., Bertolacci, M., Bowman, K. W., Carroll, D., et al. (2023). National CO₂ budgets (2015–2020) inferred from atmospheric CO₂ observations in support of the global stocktake. *Earth System Science Data*, 15(2), 963–1004. <https://doi.org/10.5194/essd-15-963-2023>
- Canadell, J. G., Ciais, P., Gurney, K., Le Quéré, C., Piao, S., Raupach, M. R., & Sabine, C. L. (2011). An international effort to quantify regional carbon fluxes. *Eos, Transactions American Geophysical Union*, 92(10), 81–82. <https://doi.org/10.1029/2011EO100001>
- Chapin, F. S., Woodwell, G. M., Randerson, J. T., Rastetter, E. B., Lovett, G. M., Baldocchi, D. D., et al. (2006). Reconciling carbon-cycle concepts, terminology, and methods. *Ecosystems*, 9(7), 1041–1050. <https://doi.org/10.1007/s10021-005-0105-7>
- Chini, L., Hurr, G., Sahajpal, R., Frolking, S., Klein Goldewijk, K., Sitch, S., et al. (2021). Land-use harmonization datasets for annual global carbon budgets. *Earth System Science Data*, 13(8), 4175–4189. <https://doi.org/10.5194/essd-13-4175-2021>
- Ciais, P., Bastos, A., Chevallier, F., Lauerwald, R., Poulter, B., Canadell, J. G., et al. (2022). Definitions and methods to estimate regional land carbon fluxes for the second phase of the REgional Carbon Cycle Assessment and Processes Project (RECCAP-2). *Geoscientific Model Development*, 15(3), 1289–1316. <https://doi.org/10.5194/gmd-15-1289-2022>
- Ciais, P., Bousquet, P., Freibauer, A., & Naegler, T. (2007). Horizontal displacement of carbon associated with agriculture and its impacts on atmospheric CO₂. *Global Biogeochemical Cycles*, 21(2). <https://doi.org/10.1029/2006GB002741>
- Ciais, P., Yao, Y., Gasser, T., Baccini, A., Wang, Y., Lauerwald, R., et al. (2021). Empirical estimates of regional carbon budgets imply reduced global soil heterotrophic respiration. *National Science Review*, 8(2), nwaal45. <https://doi.org/10.1093/nsr/nwaa145>
- Conchedda, G., & Tubiello, F. N. (2020). Drainage of organic soils and GHG emissions: Validation with country data. *Earth System Science Data*, 12(4), 3113–3137. <https://doi.org/10.5194/essd-12-3113-2020>
- Crimmins, A. R., Avery, C. W., Easterling, D. R., Kunkel, K. E., Stewart, B. C., & Maycock, T. K. (2023). *USGCRP, 2023: Fifth national climate assessment*. U.S. Global Change Research Program. <https://doi.org/10.7930/NCA5.2023>
- Deng, Z., Ciais, P., Tzompa-Sosa, Z. A., Saunio, M., Qiu, C., Tan, C., et al. (2022). Comparing national greenhouse gas budgets reported in UNFCCC inventories against atmospheric inversions. *Earth System Science Data*, 14(4), 1639–1675. <https://doi.org/10.5194/essd-14-1639-2022>
- Domke, G. M., Walters, B. F., Smith, J. E., Greenfield, E. J., Giebk, C. L., Ogle, S. M., et al. (2024). *Greenhouse gas emissions and removals from forest land, woodlands, urban trees, and harvested wood products in the United States, 1990–2022 (No. WO-RB-102)* (p. 5). U.S. Department of Agriculture, Forest Service. <https://doi.org/10.2737/WO-RB-102>
- Ernst, Y., Archibald, S., Balzter, H., Chevallier, F., Ciais, P., Fischer, C. G., et al. (2024). The african regional greenhouse gases budget (2010–2019). *Global Biogeochemical Cycles*, 38(4), e2023GB008016. <https://doi.org/10.1029/2023GB008016>
- Etioge, G., Ciotoli, G., Schwietzke, S., & Schoell, M. (2019). Gridded maps of geological methane emissions and their isotopic signature. *Earth System Science Data*, 11(1), 1–22. <https://doi.org/10.5194/essd-11-1-2019>
- Fan, L., Wigneron, J.-P., Ciais, P., Chave, J., Brandt, M., Fensholt, R., et al. (2019). Satellite-observed pantropical carbon dynamics. *Nature Plants*, 5(9), 944–951. <https://doi.org/10.1038/s41477-019-0478-9>
- Fennel, K., Alin, S. R., Barbero, L., Evans, W., Bourgeois, T., Cooley, S. R., et al. (2018). Chapter 16: Coastal ocean and continental shelves. In N. Cavallaro, G. Shrestha, R. Birdsey, M. A. Mayes, R. G. Najjar, S. C. Reed, et al. (Eds.), *Second state of the carbon cycle report (SOCCR2): A sustained assessment report* (pp. 649–688). U.S. Global Change Research Program. <https://doi.org/10.7930/Soccr2.2018.Ch16>
- Forster, P. M., Smith, C., Walsh, T., Lamb, W. F., Lamboll, R., Hall, B., et al. (2024). Indicators of global climate change 2023: Annual update of key indicators of the state of the climate system and human influence. *Earth System Science Data*, 16(6), 2625–2658. <https://doi.org/10.5194/essd-16-2625-2024>
- Friedlingstein, P., O'Sullivan, M., Jones, M. W., Andrew, R. M., Bakker, D. C. E., Hauck, J., et al. (2023). Global carbon budget 2023. *Earth System Science Data*, 15(12), 5301–5369. <https://doi.org/10.5194/essd-15-5301-2023>
- Friedlingstein, P., O'Sullivan, M., Jones, M. W., Andrew, R. M., Gregor, L., Hauck, J., et al. (2022). Global carbon budget 2022. *Earth System Science Data*, 14(11), 4811–4900. <https://doi.org/10.5194/essd-14-4811-2022>
- Friedlingstein, P., O'Sullivan, M., Jones, M. W., Andrew, R. M., Hauck, J., Olsen, A., et al. (2020). Global carbon budget 2020. *Earth System Science Data*, 12(4), 3269–3340. <https://doi.org/10.5194/essd-12-3269-2020>
- Gasser, T., Crepin, L., Quilcaille, Y., Houghton, R. A., Ciais, P., & Obersteiner, M. (2020). Historical CO₂ emissions from land use and land cover change and their uncertainty. *Biogeosciences*, 17(15), 4075–4101. <https://doi.org/10.5194/bg-17-4075-2020>

- Grassi, G., Schwingshackl, C., Gasser, T., Houghton, R. A., Sitch, S., Canadell, J. G., et al. (2023). Harmonising the land-use flux estimates of global models and national inventories for 2000–2020. *Earth System Science Data*, 15(3), 1093–1114. <https://doi.org/10.5194/essd-15-1093-2023>
- Grassi, G., Stehfest, E., Rogelj, J., van Vuuren, D., Cescatti, A., House, J., et al. (2021). Critical adjustment of land mitigation pathways for assessing countries' climate progress. *Nature Climate Change*, 11(5), 425–434. <https://doi.org/10.1038/s41558-021-01033-6>
- Guenther, A. B., Jiang, X., Heald, C. L., Sakulyanontvittaya, T., Duhl, T., Emmons, L. K., & Wang, X. (2012). The model of emissions of gases and Aerosols from nature version 2.1 (MEGAN2.1): An extended and updated framework for modeling biogenic emissions. *Geoscientific Model Development*, 5(6), 1471–1492. <https://doi.org/10.5194/gmd-5-1471-2012>
- Gurney, K. R., Liang, J., Patarasuk, R., Song, Y., Huang, J., & Roest, G. (2020). The Vulcan version 3.0 high-resolution fossil fuel CO₂ emissions for the United States. *Journal of Geophysical Research: Atmospheres*, 125(19), e2020JD032974. <https://doi.org/10.1029/2020JD032974>
- Hansen, M. C., Potapov, P. V., Moore, R., Hancher, M., Turubanova, S. A., Tyukavina, A., et al. (2013). High-resolution global maps of 21st-century forest cover change. *Science*, 342(6160), 850–853. <https://doi.org/10.1126/science.1244693>
- Hansis, E., Davis, S. J., & Pongratz, J. (2015). Relevance of methodological choices for accounting of land use change carbon fluxes. *Global Biogeochemical Cycles*, 29(8), 1230–1246. <https://doi.org/10.1002/2014GB004997>
- Harris, N. L., Gibbs, D. A., Baccini, A., Birdsey, R. A., de Bruin, S., Farina, M., et al. (2021). Global maps of twenty-first century forest carbon fluxes. *Nature Climate Change*, 11(3), 234–240. <https://doi.org/10.1038/s41558-020-00976-6>
- Harris, N. L., Hagen, S. C., Saatchi, S. S., Pearson, T. R. H., Woodall, C. W., Domke, G. M., et al. (2016). Attribution of net carbon change by disturbance type across forest lands of the conterminous United States. *Carbon Balance and Management*, 11(1), 24. <https://doi.org/10.1186/s13021-016-0066-5>
- Hartmann, J., Jansen, N., Dürr, H. H., Kempe, S., & Köhler, P. (2009). Global CO₂-consumption by chemical weathering: What is the contribution of highly active weathering regions? *Global and Planetary Change*, 69(4), 185–194. <https://doi.org/10.1016/j.gloplacha.2009.07.007>
- Hayes, D. J., Turner, D. P., Stinson, G., McGuire, A. D., Wei, Y., West, T. O., et al. (2012). Reconciling estimates of the contemporary North American carbon balance among terrestrial biosphere models, atmospheric inversions, and a new approach for estimating net ecosystem exchange from inventory-based data. *Global Change Biology*, 18(4), 1282–1299. <https://doi.org/10.1111/j.1365-2486.2011.02627.x>
- Hayes, D. J., Vargas, R., Alin, S. R., Conant, R. T., Hutyra, L. R., Jacobson, A. R., et al. (2018). Chapter 2: The North American carbon budget. In *Second state of the carbon cycle report (SOCCR2): A sustained assessment report* (pp. 71–108). U.S. Global Change Research Program. <https://doi.org/10.7930/SOCCR2.2018.Ch2>
- Houghton, R. A., & Nassikas, A. A. (2017). Global and regional fluxes of carbon from land use and land cover change 1850–2015. *Global Biogeochemical Cycles*, 31(3), 456–472. <https://doi.org/10.1002/2016GB005546>
- Hristov, A. N., Johnson, J. M. F., Rice, C. W., Brown, M. E., Conant, R. T., Del Grosso, S. J., et al. (2018). Chapter 5: Agriculture. In *Second state of the carbon cycle report (SOCCR2): A sustained assessment report* ([N. Cavallaro, G. Shrestha, R. Birdsey, M. A. Mayes, R. G. Najjar, S. C. Reed, et al. (eds.)].) (pp. 229–263). U.S. Global Change Research Program. <https://doi.org/10.7930/SOCCR2.2018.Ch5>
- Hu, L., Andrews, A. E., Thoning, K. W., Sweeney, C., Miller, J. B., Michalak, A. M., et al. (2019). Enhanced North American carbon uptake associated with El Niño. *Science Advances*, 5(6), eaaw0076. <https://doi.org/10.1126/sciadv.aaw0076>
- Hunka, N., Duncanson, L., Armston, J., Dubayah, R., Healey, S. P., Santoro, M., et al. (2024). Intergovernmental panel on climate change (IPCC) tier 1 forest biomass estimates from Earth observation. *Scientific Data*, 11(1), 1127. <https://doi.org/10.1038/s41597-024-03930-9>
- Hunka, N., Santoro, M., Armston, J., Dubayah, R., McRoberts, R. E., Næsset, E., et al. (2023). On the NASA GEDI and ESA CCI biomass maps: Aligning for uptake in the UNFCCC global stocktake. *Environmental Research Letters*, 18(12), 124042. <https://doi.org/10.1088/1748-9326/ad0b60>
- Intergovernmental Panel On Climate Change (Ipcc). (2023). *Climate change 2021 – the physical science basis: Working group I contribution to the Sixth assessment report of the intergovernmental panel on climate change* (1st ed.). Cambridge University Press. <https://doi.org/10.1017/9781009157896>
- IPCC. (2006). In H. S. Eggleston, L. Buendia, K. Miwa, T. Ngara, & K. Tanabe (Eds.), *2006 IPCC guidelines for national greenhouse gas inventories, prepared by the National Greenhouse Gas Inventories Programme*. IGES.
- IPCC. (2019). In E. Calvo Buendia, K. Tanabe, A. Kranjc, J. Baasansuren, M. Fukuda, S. Ngarize, et al. (Eds.), *2019 Refinement to the 2006 IPCC Guidelines for National Greenhouse Gas Inventories*. IPCC.
- Ito, A. (2023). Global termite methane emissions have been affected by climate and land-use changes. *Scientific Reports*, 13(1), 17195. <https://doi.org/10.1038/s41598-023-44529-1>
- Joiner, J., & Yoshida, Y. (2020). Satellite-based reflectances capture large fraction of variability in global gross primary production (GPP) at weekly time scales. *Agricultural and Forest Meteorology*, 291, 108092. <https://doi.org/10.1016/j.agrformet.2020.108092>
- King, A. W., Andres, R. J., Davis, K. J., Hafer, M., Hayes, D. J., Huntzinger, D. N., et al. (2015). North America's net terrestrial CO₂ exchange with the atmosphere 1990–2009. *Biogeosciences*, 12(2), 399–414. <https://doi.org/10.5194/bg-12-399-2015>
- Kirschke, S., Bousquet, P., Ciais, P., Saunio, M., Canadell, J. G., Dlugokencky, E. J., et al. (2013). Three decades of global methane sources and sinks. *Nature Geoscience*, 6(10), 813–823. <https://doi.org/10.1038/ngeo1955>
- Knox, S. H., Jackson, R. B., Poulter, B., McNicol, G., Fluet-Chouinard, E., Zhang, Z., et al. (2019). FLUXNET-CH4 synthesis activity: Objectives, observations, and future directions. *Bulletin of the American Meteorological Society*, 100(12), 2607–2632. <https://doi.org/10.1175/BAMS-D-18-0268.1>
- Kurz, W. A., Hayne, S., Fellows, M., MacDonald, J. D., Metsaranta, J. M., Hafer, M., & Blain, D. (2018). Quantifying the impacts of human activities on reported greenhouse gas emissions and removals in Canada's managed forest: Conceptual framework and implementation. *Canadian Journal of Forest Research*, 48(10), 1227–1240. <https://doi.org/10.1139/cjfr-2018-0176>
- Laruelle, G. G., Dürr, H. H., Lauerwald, R., Hartmann, J., Slomp, C. P., Goossens, N., & Regnier, P. A. G. (2013). Global multi-scale segmentation of continental and coastal waters from the watersheds to the continental margins. *Hydrology and Earth System Sciences*, 17(5), 2029–2051. <https://doi.org/10.5194/hess-17-2029-2013>
- Lauerwald, R., Allen, G. H., Deemer, B. R., Liu, S., Maavara, T., Raymond, P., et al. (2023a). Inland water greenhouse gas budgets for RECCAP2: 1. State-Of-The-Art of global scale assessments. *Global Biogeochemical Cycles*, 37(5), e2022GB007657. <https://doi.org/10.1029/2022GB007657>
- Lauerwald, R., Allen, G. H., Deemer, B. R., Liu, S., Maavara, T., Raymond, P., et al. (2023b). Inland water greenhouse gas budgets for RECCAP2: 2. Regionalization and homogenization of estimates. *Global Biogeochemical Cycles*, 37(5), e2022GB007658. <https://doi.org/10.1029/2022GB007658>
- Lauerwald, R., Regnier, P., Figueiredo, V., Enrich-Prast, A., Bastviken, D., Lehner, B., et al. (2019). Natural lakes are a minor global source of N₂O to the atmosphere. *Global Biogeochemical Cycles*, 33(12), 1564–1581. <https://doi.org/10.1029/2019GB006261>

- Li, X., & Xiao, J. (2019). A global, 0.05-degree product of solar-induced chlorophyll fluorescence derived from OCO-2, MODIS, and reanalysis data. *Remote Sensing*, 11(5), 517. <https://doi.org/10.3390/rs11050517>
- Liu, M., Raymond, P. A., Lauerwald, R., Zhang, Q., Trapp-Müller, G., Davis, K. L., et al. (2024). Global riverine land-to-ocean carbon export constrained by observations and multi-model assessment. *Nature Geoscience*, 17(9), 896–904. <https://doi.org/10.1038/s41561-024-01524-z>
- Liu, S., Kuhn, C., Amatulli, G., Aho, K., Butman, D. E., Allen, G. H., et al. (2022). The importance of hydrology in routing terrestrial carbon to the atmosphere via global streams and rivers. *Proceedings of the National Academy of Sciences*, 119(11), e2106322119. <https://doi.org/10.1073/pnas.2106322119>
- Liu, Z., Deng, Z., Davis, S. J., Giron, C., & Ciais, P. (2022). Monitoring global carbon emissions in 2021. *Nature Reviews Earth and Environment*, 3(4), 217–219. <https://doi.org/10.1038/s43017-022-00285-w>
- Lu, X., Jacob, D. J., Zhang, Y., Shen, L., Sulprizio, M. P., Maasakkers, J. D., et al. (2023). Observation-derived 2010–2019 trends in methane emissions and intensities from US oil and gas fields tied to activity metrics. *Proceedings of the National Academy of Sciences*, 120(17), e2217900120. <https://doi.org/10.1073/pnas.2217900120>
- Maavara, T., Lauerwald, R., Laruelle, G. G., Akbarzadeh, Z., Bouskill, N. J., Van Cappellen, P., & Regnier, P. (2019). Nitrous oxide emissions from inland waters: Are IPCC estimates too high? *Global Change Biology*, 25(2), 473–488. <https://doi.org/10.1111/gcb.14504>
- Masarie, K. A., Peters, W., Jacobson, A. R., & Tans, P. P. (2014). ObsPack: A framework for the preparation, delivery, and attribution of atmospheric greenhouse gas measurements. *Earth System Science Data*, 6(2), 375–384. <https://doi.org/10.5194/essd-6-375-2014>
- Mayorga, E., Seitzinger, S. P., Harrison, J. A., Dumont, E., Beusen, A. H. W., Bouwman, A. F., et al. (2010). Global nutrient export from WaterSheds 2 (NEWS 2): Model development and implementation. *Environmental Modelling and Software*, 25(7), 837–853. <https://doi.org/10.1016/j.envsoft.2010.01.007>
- McGlynn, E., Li, S., F. Berger, M., Amend, M., & L. Harper, K. (2022). Addressing uncertainty and bias in land use, land use change, and forestry greenhouse gas inventories. *Climatic Change*, 170(1), 5. <https://doi.org/10.1007/s10584-021-03254-2>
- McNicol, G., Fluet-Chouinard, E., Ouyang, Z., Knox, S., Zhang, Z., Aalto, T., et al. (2023). Upscaling wetland methane emissions from the FLUXNET-CH4 eddy covariance network (UpCH4 v1.0): Model development, network assessment, and budget comparison. *AGU Advances*, 4(5), e2023AV000956. <https://doi.org/10.1029/2023AV000956>
- Mcowen, C., Weatherdon, L., Bochove, J.-W., Sullivan, E., Blyth, S., Zockler, C., et al. (2017). A global map of saltmarshes. *Biodiversity Data Journal*, 5, e11764. <https://doi.org/10.3897/BDJ.5.e11764>
- Merrill, M. D., Sleeter, B. M., Freeman, P. A., Liu, J., Warwick, P. D., & Reed, B. C. (2018). *Federal lands greenhouse gas emissions and sequestration in the United States—estimates for 2005–14* (p. 31). Scientific Investigations Report.
- Messenger, M. L., Lehner, B., Grill, G., Nedeva, I., & Schmitt, O. (2016). Estimating the volume and age of water stored in global lakes using a geo-statistical approach. *Nature Communications*, 7(1), 13603. <https://doi.org/10.1038/ncomms13603>
- Moosdorf, N., Hartmann, J., Lauerwald, R., Hagedorn, B., & Kempe, S. (2011). Atmospheric CO₂ consumption by chemical weathering in North America. *Geochimica et Cosmochimica Acta*, 75(24), 7829–7854. <https://doi.org/10.1016/j.gca.2011.10.007>
- Mörner, N.-A., & Etiope, G. (2002). Carbon degassing from the lithosphere. *Global and Planetary Change*, 33(1), 185–203. [https://doi.org/10.1016/S0921-8181\(02\)00070-X](https://doi.org/10.1016/S0921-8181(02)00070-X)
- Murray-Tortarolo, G., Poulter, B., Vargas, R., Hayes, D., Michalak, A. M., Williams, C., et al. (2022). A process-model perspective on recent changes in the carbon cycle of North America. *Journal of Geophysical Research: Biogeosciences*, 127(9), e2022JG006904. <https://doi.org/10.1029/2022JG006904>
- Nusser, S. M. (2012). National Resources inventory (NRI), US. In A. H. El-Shaarawi & W. W. Piegorsch (Eds.), *Encyclopedia of environmetrics* (1st ed.). Wiley. <https://doi.org/10.1002/9780470057339.van004.pub2>
- Obermeier, W. A., Nabel, J. E. M. S., Loughran, T., Hartung, K., Bastos, A., Havemann, F., et al. (2021). Modelled land use and land cover change emissions – A spatio-temporal comparison of different approaches. *Earth System Dynamics*, 12(2), 635–670. <https://doi.org/10.5194/esd-12-635-2021>
- Ogle, S. M., Domke, G., Kurz, W. A., Rocha, M. T., Huffman, T., Swan, A., et al. (2018). Delineating managed land for reporting national greenhouse gas emissions and removals to the United Nations framework convention on climate change. *Carbon Balance and Management*, 13(1), 9. <https://doi.org/10.1186/s13021-018-0095-3>
- Pacala, S. W., Hurtt, G. C., Baker, D., Peylin, P., Houghton, R. A., Birdsey, R. A., et al. (2001). Consistent land- and atmosphere-based U.S. Carbon sink estimates. *Science*, 292(5525), 2316–2320. <https://doi.org/10.1126/science.1057320>
- Peng, S., Lin, X., Thompson, R. L., Xi, Y., Liu, G., Hauglustaine, D., et al. (2022). Wetland emission and atmospheric sink changes explain methane growth in 2020. *Nature*, 612(7940), 477–482. <https://doi.org/10.1038/s41586-022-05447-w>
- Peters, G. P., Davis, S. J., & Andrew, R. (2012). A synthesis of carbon in international trade. *Biogeosciences*, 9(8), 3247–3276. <https://doi.org/10.5194/bg-9-3247-2012>
- Petrescu, A. M. R., McGrath, M. J., Andrew, R. M., Peylin, P., Peters, G. P., Ciais, P., et al. (2021). The consolidated European synthesis of CO₂ emissions and removals for the European union and United Kingdom: 1990–2018. *Earth System Science Data*, 13(5), 2363–2406. <https://doi.org/10.5194/essd-13-2363-2021>
- Petrescu, A. M. R., Qiu, C., McGrath, M. J., Peylin, P., Peters, G. P., Ciais, P., et al. (2023). The consolidated European synthesis of CH₄ and N₂O emissions for the European union and United Kingdom: 1990–2019. *Earth System Science Data*, 15(3), 1197–1268. <https://doi.org/10.5194/essd-15-1197-2023>
- Poggio, L., De Sousa, L. M., Batjes, N. H., Heuvelink, G. B. M., Kempen, B., Ribeiro, E., & Rossiter, D. (2021). SoilGrids 2.0: Producing soil information for the globe with quantified spatial uncertainty. *SOIL*, 7(1), 217–240. <https://doi.org/10.5194/soil-7-217-2021>
- Pongratz, J., Schwingshackl, C., Bultan, S., Obermeier, W., Havemann, F., & Guo, S. (2021). Land use effects on climate: Current state, recent progress, and emerging topics. *Current Climate Change Reports*, 7(4), 99–120. <https://doi.org/10.1007/s40641-021-00178-y>
- Poulter, B. (2025). The North American greenhouse gas budget: Emissions, removals, and integration for CO₂, CH₄, and N₂O (2010–2019): Results from the second REgional carbon cycle assessment and processes study (RECCAP2) (version 1) [Dataset]. *Zenodo*. <https://doi.org/10.5281/ZENODO.14940052>
- Poulter, B., Bastos, A., Canadell, J. G., Ciais, P., Gruber, N., Hauck, J., et al. (2022). Inventorying Earth's land and Ocean greenhouse gases. *Eos*, 103. <https://doi.org/10.1029/2022eo179084>
- Poulter, B., Bousquet, P., Canadell, J. G., Ciais, P., Peregón, A., Saunio, M., et al. (2017). Global wetland contribution to 2000–2012 atmospheric methane growth rate dynamics. *Environmental Research Letters*, 12(9), 094013. <https://doi.org/10.1088/1748-9326/aa8391>
- Ramo, R., Roteta, E., Bistinas, I., Van Wees, D., Bastarrika, A., Chuvieco, E., & Van Der Werf, G. R. (2021). African burned area and fire carbon emissions are strongly impacted by small fires undetected by coarse resolution satellite data. *Proceedings of the National Academy of Sciences*, 118(9), e2011160118. <https://doi.org/10.1073/pnas.2011160118>

- Raymond, P. A., Hartmann, J., Lauerwald, R., Sobek, S., McDonald, C., Hoover, M., et al. (2013). Global carbon dioxide emissions from inland waters. *Nature*, 503(7476), 355–359. <https://doi.org/10.1038/nature12760>
- Regnier, P., Friedlingstein, P., Ciais, P., Mackenzie, F. T., Gruber, N., Janssens, I. A., et al. (2013). Anthropogenic perturbation of the carbon fluxes from land to ocean. *Nature Geoscience*, 6(8), 597–607. <https://doi.org/10.1038/ngeo1830>
- Regnier, P., Resplandy, L., Najjar, R. G., & Ciais, P. (2022). The land-to-ocean loops of the global carbon cycle. *Nature*, 603(7901), 401–410. <https://doi.org/10.1038/s41586-021-04339-9>
- Resplandy, L., Hogikyan, A., Müller, J. D., Najjar, R. G., Bange, H. W., Bianchi, D., et al. (2024). A synthesis of global coastal ocean greenhouse gas fluxes. *Global Biogeochemical Cycles*, 38(1), e2023GB007803. <https://doi.org/10.1029/2023GB007803>
- Resplandy, L., Keeling, R. F., Eddebbar, Y., Brooks, M. K., Wang, R., Bopp, L., et al. (2018). Quantification of ocean heat uptake from changes in atmospheric O₂ and CO₂ composition. *Nature*, 563(7729), 105–108. <https://doi.org/10.1038/s41586-018-0651-8>
- Rocher-Ros, G., Stanley, E. H., Loken, L. C., Casson, N. J., Raymond, P. A., Liu, S., et al. (2023). Global methane emissions from rivers and streams. *Nature*, 621(7979), 530–535. <https://doi.org/10.1038/s41586-023-06344-6>
- Rodríguez-Fernández, N. J., Mialon, A., Mermoz, S., Bouvet, A., Richaume, P., Al Bitar, A., et al. (2018). An evaluation of SMOS L-band vegetation optical depth (L-VOD) data sets: High sensitivity of L-VOD to above-ground biomass in Africa. *Biogeosciences*, 15(14), 4627–4645. <https://doi.org/10.5194/bg-15-4627-2018>
- Rosentreter, J. A., Laruelle, G. G., Bange, H. W., Bianchi, T. S., Busecke, J. J. M., Cai, W.-J., et al. (2023). Coastal vegetation and estuaries are collectively a greenhouse gas sink. *Nature Climate Change*, 13(6), 579–587. <https://doi.org/10.1038/s41558-023-01682-9>
- Salazar-Neira, J. C., Mialon, A., Richaume, P., Mermoz, S., Kerr, Y. H., Bouvet, A., et al. (2023). Above-Ground biomass estimation based on multi-angular L-band measurements of brightness temperatures. *Ieee Journal of Selected Topics in Applied Earth Observations and Remote Sensing*, 16, 5813–5827. <https://doi.org/10.1109/JSTARS.2023.3285288>
- Santoro, M., Cartus, O., Carvalhais, N., Rozendaal, D. M. A., Avitabile, V., Araza, A., et al. (2021). The global forest above-ground biomass pool for 2010 estimated from high-resolution satellite observations. *Earth System Science Data*, 13(8), 3927–3950. <https://doi.org/10.5194/essd-13-3927-2021>
- Saunois, M., Martinez, A., Poulter, B., Zhang, Z., Raymond, P., Regnier, P., et al. (2024). Global methane budget 2000–2020. <https://doi.org/10.5194/essd-2024-115>
- Saunois, M., Stavert, A. R., Poulter, B., Bousquet, P., Canadell, J. G., Jackson, R. B., et al. (2020). The global methane budget 2000–2017. *Earth System Science Data*, 12(3), 1561–1623. <https://doi.org/10.5194/essd-12-1561-2020>
- Schulze, E. D., Ciais, P., Luyssaert, S., Schrumpp, M., Janssens, I. A., Thiruchittampalam, B., et al. (2010). The European carbon balance. Part 4: Integration of carbon and other trace-gas fluxes. *Global Change Biology*, 16(5), 1451–1469. <https://doi.org/10.1111/j.1365-2486.2010.02215.x>
- Schulze, E. D., Luyssaert, S., Ciais, P., Freibauer, A., Janssens, I. A., Soussana, J. F., et al. (2009). Importance of methane and nitrous oxide for Europe's terrestrial greenhouse-gas balance. *Nature Geoscience*, 2(12), 842–850. <https://doi.org/10.1038/ngeo686>
- Schwingshackl, C., Obermeier, W. A., Bultan, S., Grassi, G., Canadell, J. G., Friedlingstein, P., et al. (2022). Differences in land-based mitigation estimates reconciled by separating natural and land-use CO₂ fluxes at the country level. *One Earth*, 5(12), 1367–1376. <https://doi.org/10.1016/j.oneear.2022.11.009>
- Sindelarova, K., Markova, J., Simpson, D., Huszar, P., Karlicky, J., Darras, S., & Granier, C. (2022). High-resolution biogenic global emission inventory for the time period 2000–2019 for air quality modelling. *Earth System Science Data*, 14(1), 251–270. <https://doi.org/10.5194/essd-14-251-2022>
- Sitch, S., Friedlingstein, P., Gruber, N., Jones, S. D., Murray-Tortarolo, G., Ahlström, A., et al. (2015). Recent trends and drivers of regional sources and sinks of carbon dioxide. *Biogeosciences*, 12(3), 653–679. <https://doi.org/10.5194/bg-12-653-2015>
- Stavert, A. R., Saunois, M., Canadell, J. G., Poulter, B., Jackson, R. B., Regnier, P., et al. (2022). Regional trends and drivers of the global methane budget. *Global Change Biology*, 28(1), 182–200. <https://doi.org/10.1111/gcb.15901>
- Stell, E., Warner, D., Jian, J., Bond-Lamberty, B., & Vargas, R. (2021). Global gridded 1-km soil and soil heterotrophic respiration derived from SRDB v5 [Dataset]. *Oak Ridge, Tennessee, USA*. <https://doi.org/10.3334/ORNLDAAAC/1928>
- Tian, H., Pan, N., Thompson, R. L., Canadell, J. G., Suntharalingam, P., Regnier, P., et al. (2024). Global nitrous oxide budget (1980–2020). *Earth System Science Data*, 16(6), 2543–2604. <https://doi.org/10.5194/essd-16-2543-2024>
- Tian, H., Xu, R., Canadell, J. G., Thompson, R. L., Winiwarter, W., Suntharalingam, P., et al. (2020). A comprehensive quantification of global nitrous oxide sources and sinks. *Nature*, 586(7828), 248–256. <https://doi.org/10.1038/s41586-020-2780-0>
- Tian, H., Xu, X., Liu, M., Ren, W., Zhang, C., Chen, G., & Lu, C. (2010). Spatial and temporal patterns of CH₄ and N₂O fluxes in terrestrial ecosystems of North America during 1979–2008: Application of a global biogeochemistry model. *Biogeosciences*, 7(9), 2673–2694. <https://doi.org/10.5194/bg-7-2673-2010>
- Tramontana, G., Jung, M., Schwalm, C. R., Ichii, K., Camps-Valls, G., Ráduly, B., et al. (2016). Predicting carbon dioxide and energy fluxes across global FLUXNET sites with regression algorithms. *Biogeosciences*, 13(14), 4291–4313. <https://doi.org/10.5194/bg-13-4291-2016>
- Tubiello, F. N., Conchedda, G., Wanner, N., Federici, S., Rossi, S., & Grassi, G. (2021). Carbon emissions and removals from forests: New estimates, 1990–2020. *Earth System Science Data*, 13(4), 1681–1691. <https://doi.org/10.5194/essd-13-1681-2021>
- UNEP-WCMC, & Short, F. T. (2005). *Global distribution of seagrasses (version 7.1) [WMS; KML (.kml); vector (polygon); vector (point)]*. United Nations Environment Programme World Conservation Monitoring Centre (UNEP-WCMC). <https://doi.org/10.34892/X6R3-D211>
- Van Der Werf, G. R., Randerson, J. T., Collatz, G. J., & Giglio, L. (2003). Carbon emissions from fires in tropical and subtropical ecosystems. *Global Change Biology*, 9(4), 547–562. <https://doi.org/10.1046/j.1365-2486.2003.00604.x>
- van der Werf, G. R., Randerson, J. T., Giglio, L., Collatz, G. J., Mu, M., Kasibhatla, P. S., et al. (2010). Global fire emissions and the contribution of deforestation, savanna, forest, agricultural, and peat fires (1997–2009). *Atmospheric Chemistry and Physics*, 10(23), 11707–11735. <https://doi.org/10.5194/acp-10-11707-2010>
- Villalobos, Y., Canadell, J. G., Keller, E. D., Briggs, P. R., Bukosa, B., Giltrap, D. L., et al. (2023). A comprehensive assessment of anthropogenic and natural sources and sinks of Australasia's carbon budget. *Global Biogeochemical Cycles*, 37(12), e2023GB007845. <https://doi.org/10.1029/2023GB007845>
- Vörösmarty, C. J., Fekete, B. M., Meybeck, M., & Lammers, R. B. (2000). Global system of rivers: Its role in organizing continental land mass and defining land-to-ocean linkages. *Global Biogeochemical Cycles*, 14(2), 599–621. <https://doi.org/10.1029/1999GB900092>
- Wang, X., Gao, Y., Jeong, S., Ito, A., Bastos, A., Poulter, B., et al. (2024). The greenhouse gas budget of terrestrial ecosystems in East Asia since 2000. *Global Biogeochemical Cycles*, 38(2), e2023GB007865. <https://doi.org/10.1029/2023GB007865>
- Wei, X., Zhao, J., Hayes, D. J., Daigneault, A., & Zhu, H. (2023). A life cycle and product type based estimator for quantifying the carbon stored in wood products. *Carbon Balance and Management*, 18(1), 1. <https://doi.org/10.1186/s13021-022-00220-y>
- West, T. O., Marland, G., Singh, N., Bhaduri, B. L., & Roddy, A. B. (2009). The human carbon budget: An estimate of the spatial distribution of metabolic carbon consumption and release in the United States. *Biogeochemistry*, 94(1), 29–41. <https://doi.org/10.1007/s10533-009-9306-z>

- Zhang, Z., Fluet-Chouinard, E., Jensen, K., McDonald, K., Hugelius, G., Gumbrecht, T., et al. (2021). Development of the global dataset of wetland area and dynamics for methane modeling (WAD2M). *Earth System Science Data*, 13(5), 2001–2023. <https://doi.org/10.5194/essd-13-2001-2021>
- Zhang, Z., Poulter, B., Melton, J. R., Riley, W. J., Allen, G. H., Beerling, D. J., et al. (2024). Ensemble estimates of global wetland methane emissions over 2000–2020. <https://doi.org/10.5194/egusphere-2024-1584>
- Zhao, M., Heinsch, F. A., Nemani, R. R., & Running, S. W. (2005). Improvements of the MODIS terrestrial gross and net primary production global data set. *Remote Sensing of Environment*, 95(2), 164–176. <https://doi.org/10.1016/j.rse.2004.12.011>
- Zscheischler, J., Mahecha, M. D., Avitabile, V., Calle, L., Carvalhais, N., Ciais, P., et al. (2017). Reviews and syntheses: An empirical spatio-temporal description of the global surface–atmosphere carbon fluxes: Opportunities and data limitations. *Biogeosciences*, 14(15), 3685–3703. <https://doi.org/10.5194/bg-14-3685-2017>